Using temperature to analyse the neural basis of a latent temporal decision

Tiago Monteiro[1,2,*], Filipe S. Rodrigues[1,*], Margarida Pexirra[1,3,*], Bruno F. Cruz[1], Ana I. Gonçalves[1], Pavel E. Rueda-Orozco[4], Joseph J. Paton[1,5,†]

[1] Champalimaud Centre for the Unknown, Lisbon, Portugal.
[2] Current address: Department of Zoology, University of Oxford, UK.
[3] Current address: Sainsbury Wellcome Centre for Neural Circuits and Behaviour, University College London, London, UK.
[4] Institute of Neurobiology, UNAM Juriquilla, Mexico.
[5] Lead contact
* These authors contributed equally to the work
† To whom correspondence should be addressed, joe.paton@neuro.fchampalimaud.org

SUMMARY

The basal ganglia (BG) are thought to contribute to decision-making and motor control by learning to select actions based on consequences. These functions are critically dependent on timing information that can be extracted from the evolving state of neural populations in the striatum, the major input area of the BG. However, it is debated whether striatal activity underlies latent, dynamic decision processes or kinematics of overt movement. Here, we measured the impact of temperature on striatal population activity and the behavior of rats and compared the observed effects to neural activity and behavior collected in multiple versions of a temporal categorization task. Cooler temperatures caused dilation, and warmer temperatures contraction, of both neural activity and patterns of judgment in time, mimicking endogenous decision-related variability in striatal activity. However, temperature did not similarly affect movement kinematics. These data demonstrate that the time-course of evolving striatal population activity dictates the speed of a latent process that is used to guide decision-making, but not finer temporal aspects of movement. More broadly, they establish temporal scaling of population activity as a cause and not simply a correlate of timing in the brain.

KEYWORDS

Basal ganglia, cooling, decision-making, hierarchical control, interval timing, population dynamics, striatum, temperature, temporal scaling

INTRODUCTION

Much of behavior is dependent on time. Humans and other animals must extract temporal structure from the environment to learn to anticipate events, to understand relationships between actions and consequences, and estimate time to plan and properly sequence and coordinate action. For tasks as varied as waiting at a stoplight to a hummingbird foraging for nectar, time is fundamental.

Timing mechanisms appear to be distributed across the nervous system, reflecting the importance of time information for much of brain function (Coull, Cheng and Meck, 2011; Paton and Buonomano, 2018). However, one common requirement among diverse functions is the need to create an index, ordering and spacing information along the temporal dimension such that useful relations can be extracted and outputs appropriately coordinated. On the scale of seconds to minutes at which much of behavior unfolds, neuronal population dynamics represent a candidate means of both encoding and generating temporal patterns. Artificial neural network models have explored evolving population activity as a basis for timing sensory events (Buonomano and Merzenich, 1995) and movements (Wang *et al.*, 2017). And correlations between behavior and the time-course of population activity have lent some support to the hypothesis that time-varying patterns of activity within a population perform temporal computations (Kim *et al.*, 2013; Jazayeri and Shadlen, 2015; Bakhurin *et al.*, 2017; Merchant and Averbeck, 2017). However, correlations do not imply causation. The critical prediction of these "population clock" hypotheses is that slowing or speeding the temporal evolution of activity should cause a corresponding dilation or contraction of the temporal functions performed using that activity.

One brain system where time information appears to be critical is the basal ganglia (BG), an evolutionarily ancient set of brain structures thought to contribute to appropriate action selection based on experience. A dominant view holds that the BG embed core features of reinforcement learning (RL) (Doya, 1999) algorithms. In mammals, inputs from a diverse set of territories in cortex, thalamus, and limbic brain structures convey information about the state of the world that converges with dense dopaminergic innervation in the major input area of the BG, the striatum. The input from dopamine neurons is thought to teach striatal circuits about the value of taking particular actions in a given state, information that can ultimately be conveyed to downstream brainstem and thalamo-cortical motor circuits to bias selection or otherwise specify features of actions. To accomplish such a function, the BG would need access to information about ordering and spacing along the temporal dimension both to extract meaningful relations between the environment, actions and outcomes that drive learning (Gallistel and Gibbon, 2000; Daw, Courville and Touretzky, 2006), and to coordinate the production of actions in time (Graybiel, 1998; Hidalgo-Balbuena *et al.*, 2019). Interestingly, data from people with BG disorders (Freeman *et al.*, 1996; Malapani *et al.*, 1998) and human fMRI (Rao, Mayer and Harrington, 2001; Coull *et al.*, 2004) have consistently identified the BG as being involved in timing behavior. In addition, lesions and pharmacological manipulations of the striatum can cause deficits in temporal estimation and reproduction (Meck, 2006; Mello, Soares and Paton, 2015). Lastly, recordings from striatal populations have demonstrated that time information can be decoded from neural activity, and this information correlates with variability in timing behavior (Matell, Meck and Nicolelis, 2003; Jin, Fujii and Graybiel, 2009; Gouvêa *et al.*, 2015; Bakhurin *et al.*, 2017; Kim, Kim and Jung, 2018). Specifically, the state of striatal population activity continuously changes along reproducible trajectories during behavioral tasks that require time estimation, advancing more quickly when animals report longer time estimates, and more slowly

1

when they report shorter time estimates (Gouvêa *et al.*, 2015; Mello, Soares and Paton, 2015; Bakhurin *et al.*, 2017; Wang *et al.*, 2017).

To test whether variability in the speed of BG population dynamics merely correlates with or directly regulates timing function, we sought to experimentally manipulate dynamics as animals reported temporal judgments. Interestingly, despite being composed of elements with differing temperature dependencies (Robertson and Money, 2012), neural circuits in at least some systems can produce patterns of activity that systematically slow down or speed up with decreasing or increasing temperature (Tang *et al.*, 2010; Hamaguchi, Tanaka and Mooney, 2016). For this reason, temperature manipulations offer a potential method to test hypotheses regarding the relationship between the speed of neural dynamics and function (Banerjee, Egger and Long, 2021). Indeed temperature manipulations in the zebra finch have been used to identify area HVC as a locus within the song production circuit that contributes to the temporal patterning of bird song (Long and Fee, 2008). Similar temperature manipulations in humans have identified a subregion of speech motor cortex that regulates the speed of speech (Long *et al.*, 2016), a region of rodent medial frontal cortex that controls the timing of a delayed movement (Xu *et al.*, 2014), and cooling the medial septum has been shown to slow theta oscillations in the hippocampus (Petersen and Buzsáki, 2020). However, to our knowledge, the effect of temperature on non-oscillating population trajectories has not been examined directly.

Here, we used a custom thermoelectric device (TED) to systematically vary the temperature of striatal tissue, both warming and cooling relative to a baseline condition. We found that temperature caused a bidirectional and graded change in the time-course of neural population activity in rats, resulting in systematic changes in the encoding of temporal information. These temperature dependent changes in activity mimicked decision-related variability in endogenous patterns of activity observed during multiple versions of a temporal judgment task. Lastly, varying striatal temperature caused bidirectional and graded changes in animals' timing judgments, with warmer (cooler) temperatures leading to relative overestimation (underestimation) of duration. Strikingly, these results were not accompanied by similar effects of temperature on finer timing of movement execution. Together, these findings demonstrate that the temporal evolution of the activity of populations of BG neurons can control the temporal scaling of decision variables that are used to guide judgments of duration, but not the lower level timing of how movements are executed, providing insight into how the BG may extract temporal information from the environment and use it to coordinate behavior.

RESULTS

Striatal temperature systematically modified neural population speed

Temperature has been shown in some systems to alter the speed of neural population activity while maintaining its general pattern (Tang *et al.*, 2010; Hamaguchi, Tanaka and Mooney, 2016). Thus, we first examined the effect of temperature on striatal neural activity.

First, we developed a thermoelectric device (TED) (Aronov and Fee, 2011) (**Fig. 1A**) based on the Peltier effect and used it to achieve closed-loop control over the temperature of silver metal probes implanted in brain tissue. To characterize the spatio-temporal profile of temperature changes in the brain, we measured temperature at different distances from the tip of a probe implanted in dorsal striatum (DS), setting our TED to a control level approximating normal body temperature, one warm condition or two levels of cooling (**Fig. 1E**). Throughout all experiments in the study, we

applied temperature manipulations using a block design of control-manipulation-control with transitions occurring at regular three-minute intervals (**Fig. 1E**). Manipulation temperatures were drawn at random and without replacement from the aforementioned set until its exhaustion, at which point the set was replenished and the sampling process resumed. We found that temperature near the tips of the probes tracked block changes, reaching asymptote within ~60 s of transitions (**Fig. 1E, S1B,C**), and that temperature changes fell off to minimal levels within 6 mm of the probe tip (**Fig. S1E,F**). This *in vivo* characterization of the implant confirmed that temperature manipulations were largely localized to striatal tissue and that manipulation blocks of three minute duration would allow for assessing effects of striatal temperature on neural activity and behavior.
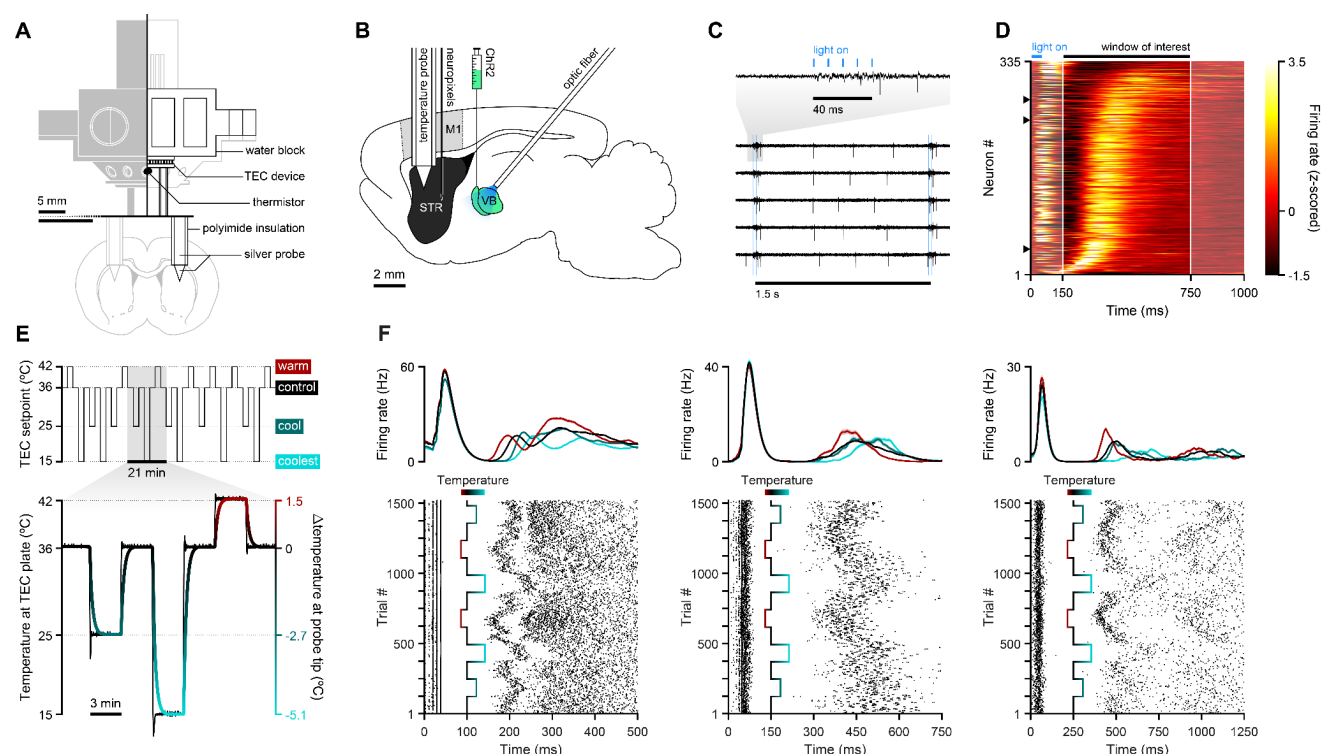
Figure 1. Temperature rescaled single striatal neuron responses in time. (**A**) Schematic of the thermoelectric device (TED). The thick horizontal line splits the diagram into two differently scaled subregions (see 5 mm scale bars). Top region is subdivided in the middle between a front view (to its left, with white strokes and gray fills) and a cutaway through the center of the implant. (**B**) Schematic of the preparation used to elicit, record and manipulate reproducible striatal dynamics under different temperatures. (**C**) VB thalamic stimulation protocol overlaid with five single-trial examples of evoked striatal voltage signals recorded in the control temperature condition. Blue ticks depict light pulses. (**D**) Normalized and smoothed peri-stimulus time histograms (PSTHs) of recorded striatal neurons (N = 335), under the control temperature. Units are ordered by their angular position in the subspace defined by the first 2 PCs describing firing dynamics between 150 ms and 750 ms from stimulation onset. This time window is delimited by white vertical lines and adjacent transparent patches. Arrowheads indicate example units shown in (F). (**E**) Top panel depicts the target setpoint of the peltier device over a representative session. Bottom panel depicts a representative segment of thermistor readings (black trace) at the lower plate of the TEC module shown in (A), illustrating the temperature manipulation protocol throughout experiments. Gradient-colored trace indicates the temperature as estimated from *in vivo* calibration experiments (**Fig. S1**). (**F**) Activity of three putative striatal units aligned to the onset of VB stimulation. Top: smoothed PSTHs split by temperature (mean ± s.e.m.). Bottom: Raster plots, wherein rows correspond to chronologically ordered trials and each tick mark to a unit-assigned action potential. The superimposed gradient-colored trace indicates temperature setpoint changed over the course of the recording session.

3

Next we characterized the features of neural activity that were affected by temperature, adapting a paradigm for optogenetically inducing patterns of striatal activity under anesthesia (Hidalgo-Balbuena *et al.*, 2019). The optogenetic approach allowed us to generate large numbers of highly reproducible bouts of population activity free from behavior-driven variability, and was thus ideal for studying the direct effects of temperature on striatal activity. Briefly, we used a viral strategy to express Channelrhodopsin-2 (ChR-2) in the ventrobasal complex (VB, **Fig. 1B**), a somatosensory thalamic area that both projects directly to the striatum, and indirectly may influence striatal activity through thalamocortical projections. Three weeks post-infection, under urethane anaesthesia, we implanted an optic fiber over VB, a single insulated silver probe of our TED into DS and an adjacent Neuropixels (Jun *et al.*, 2017) silicon probe (**Fig. 1B**, **Fig. S2A,B**). We then delivered 50-ms trains of blue light pulses at 100 Hz once every 1.5 s and recorded DS neural activity (**Fig. 1C,D**). Stimulation caused a brief volley of striatal activity, followed shortly thereafter by reproducible patterns of firing across the population over hundreds of milliseconds after the last light pulse had been delivered (**Fig. 1D**). For assessing the effect of temperature on neural responses we focused on this longer lasting activity because, unlike the initial volley, later responses reflected ongoing dynamics of the system as opposed to the direct response to stimulation.

While the general patterning of neural activity over time was maintained across different temperatures, the time-course of this pattern systematically varied depending on temperature, advancing more slowly the colder the temperature, and more quickly when temperature was raised above baseline (**Fig. 1F**). To quantify temperature dependent warping in the time-course of neural responses, we computed a scaling factor for each neuron in each of the four temperature conditions (see methods, **Fig. S3A**). Scaling as opposed to time shifting of responses provided a significantly better explanation of the effect of temperature on firing rates across the population (**Fig. S3**). For ease of comparison with behavioral effects of temperature, we transformed individual neuron scaling factors to be expressed as the percent dilation caused by each temperature (with negative values corresponding to contraction). Across all recorded neurons, distributions of percent dilation were ordered inversely as a function of temperature (**Fig. 2A**, **B**), with the majority of cells exhibiting time-contracted firing profiles (dilation < 0%) under warming, and time-dilated firing profiles (dilation > 0%) under cooling conditions. At a population level this led to systematic differences in the speed with which population state advanced along its typical trajectory in neural state space (**Fig. 2D**). Temperature also modified baseline firing rate of striatal neurons, however, this effect was distinct from the effect on temporal scaling. Whereas temperature produced a monotonic effect on temporal scaling across the sampled temperatures, baseline firing rates varied non-monotonically as a function of temperature, with both warming and cooling of striatal tissue relative to a physiologically normal control value resulting in lower firing rates (**Fig. 2C**).

Previous studies have shown that estimates of elapsed time decoded from striatal populations can predict timing judgments (Gouvêa *et al.*, 2015; Kim, Kim and Jung, 2018). To assess whether temperature effects resembled endogenous, decision-related variability in population activity during behavior and its impact on the readout of decision variables, we decoded elapsed time from the population under different temperatures. Briefly, we first characterized the "typical" temporal profiles of striatal responses using a subset of control trials, and then applied a probabilistic decoding approach to estimate elapsed time based only on the observed state of the recorded population in remaining trials. Estimates of elapsed time derived from ongoing population activity systematically led ahead and lagged behind true time during warming and cooling blocks, respectively. This can be observed by sampling the output of the decoder at discrete delays from

stimulation onset (**Fig. 2E**), and more continuously by subtracting decoder output during control blocks from that during the three different manipulation conditions (**Fig. 2F**). Relative to control, cooler temperatures gradually shifted decoded estimates of time earlier, and the warmer temperature shifted decoded estimates of time later. These data demonstrate that the temporal scaling of neural response profiles by temperature recapitulated features of endogenous variability in the time-course of population activity and time encoding in a manner previously shown to correlate with timing judgments.
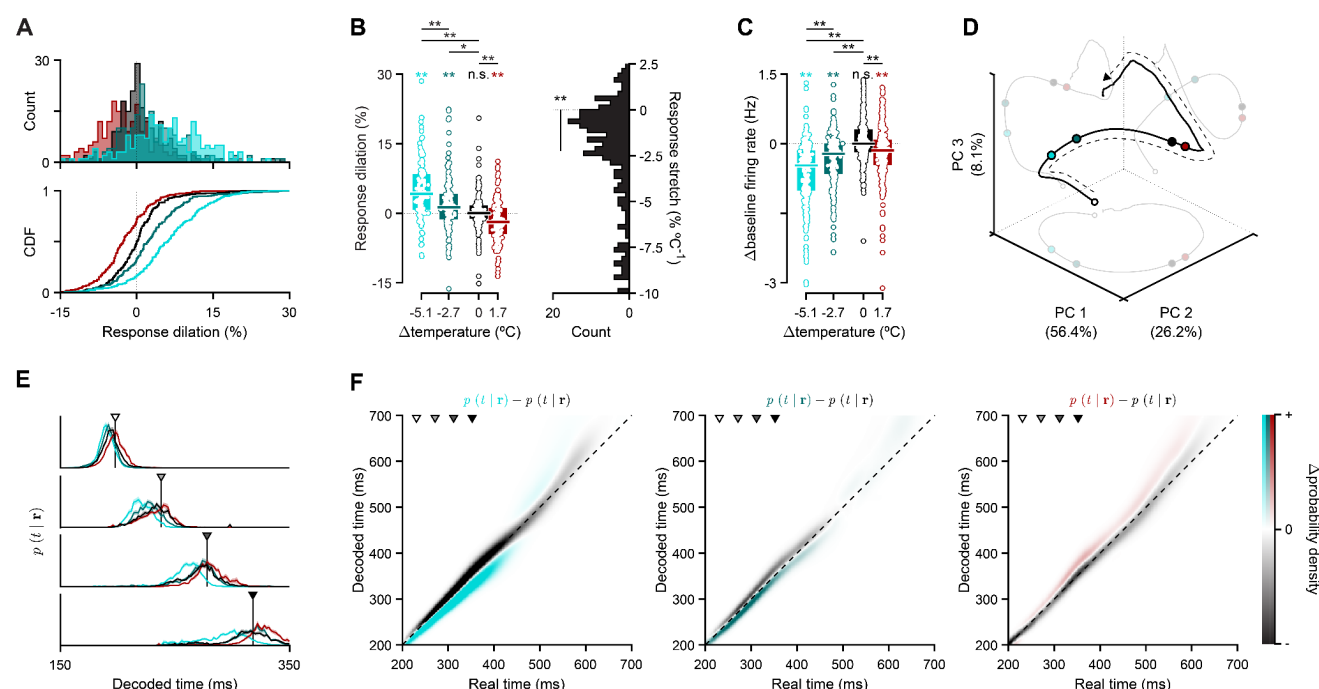
Figure 2. Temperature rescaled neural population activity in time leading to graded modulation of decoded time estimates. (**A**) Distribution of percentage change in temporal scale relative to control (dilation, N = 251, see methods). Histograms (top) and corresponding cumulative density functions (CDF, bottom) of dilation conditioned on manipulation temperature (same color scheme as in **Fig. 1**). (**B**) Left: Distributions of neuronal response dilations as a function of striatal temperature change. Markers represent temperature-split response dilations for each cell. Boxplots show population medians (horizontal thick lines) and i.q.r. (colored bars). Right: Distribution of stretch in neuronal responses. (**C**) Markers represent temperature-split change in baseline firing rate for each cell. Boxplots show population medians (horizontal thick lines) and i.q.r. (colored bars). (**D**) Average control population activity projected onto its first 3 principal components (solid black line), and temperature-split averages (colored markers) projected onto that control trajectory at the time point indicated by the last arrowhead in (E) and (F). Ghosted versions of these visualizations show their 2D projections onto all possible combinations of PCs 1, 2 and 3. The dashed black arrow indicates the direction of time. (**E**) Decoded posterior probability of time given the state of striatal populations at the time points indicated by the arrowheads in (F), averaged separately across trials for each temperature condition (mean ± s.e.m.). (**F**). Difference between decoded estimates for manipulation (left: extreme cooling; middle: mild cooling; right: warming) and control conditions, shown for the time window highlighted in **Fig. 1D**. Grayscale arrowheads indicate time points used in panel (E). The identity line is shown in dashed black.

Striatal population speed predicts temporal judgment across tasks with different immobility requirements

A number of studies have observed that ongoing behavior may correlate with timing performance (Killeen and Fetterman, 1993; Machado, Malheiro and Erlhagen, 2009; Gouvêa *et al.*, 2014; Kawai *et al.*, 2015; Safaie *et al.*, 2020). This raises the possibility that previously observed correlations between the speed of neural population activity and timing judgments might reflect the encoding of kinematic features by striatal populations (Rueda-Orozco and Robbe, 2015; Dhawale *et al.*, 2021) combined with the adoption of embodied strategies for timing (Killeen and Fetterman, 1988). Such a scenario may indicate a more indirect role for striatal population dynamics in the decision process. To examine this possibility, we studied DS population dynamics (**Fig. S2C**, **D**) during behavior in two versions of a temporal discrimination task that differed in the degree to which animals were free to move around the behavioral box during interval estimation.
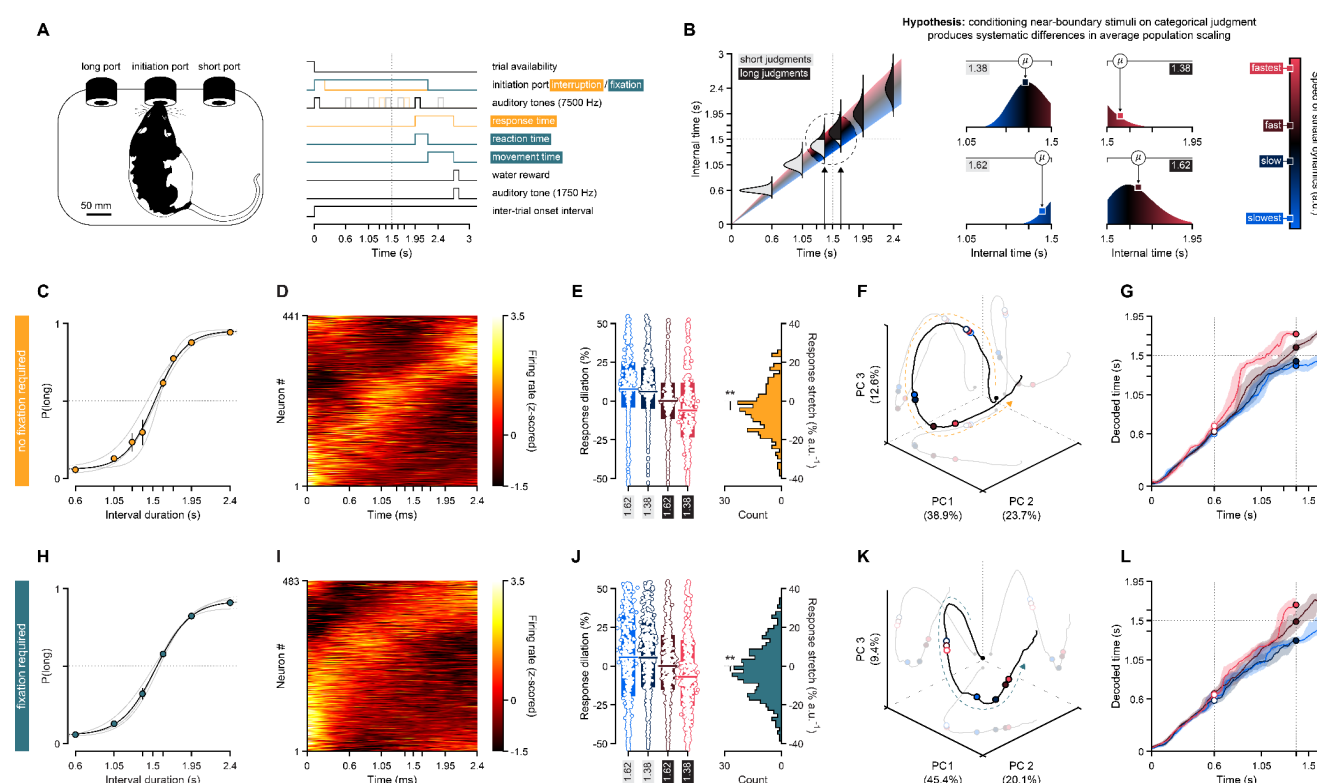
Figure 3. Conditioning neural activity on behavior produced parametric modulation of population speed and decoded estimates of elapsed time. (**A**) Schematic of behavioral setup (left) and event diagram highlighting a correct trial in both the *no fixation required* (orange) and *fixation required* (blue-green) versions of the interval discrimination task. (**B**) Left: schematic of hypothetical relationship between trial to trial variability in the speed of internal timing, blue indicating slower, and red indicating faster internal time estimates, and the resulting distributions of time estimates at each interval offset. Assuming a fixed internal decision boundary, long or short judgments are colored as black or grey portions of the distributions. Right: schematic depicting hypothetical, graded shifts in average internal timing speeds when conditioning on choice for the two intervals nearest to the decision boundary. Specifically, short (long) stimuli incorrectly categorized as long (short) should reflect pronounced biases towards faster (slower) than usual dynamics, and correctly categorized short (long) stimuli should reflect milder biases towards slower (faster) dynamics. (**C**) Performance in the *no fixation required* version of the task (N = 3). (**D**) Normalized and smoothed PSTHs of all striatal neurons (N = 441)

recorded during presentations of the longest stimulus in our set (2.4 s). Units are ordered by their angular position in the subspace defined by the first 2 PCs describing firing dynamics. (**E**) Left: Distributions of neuronal response dilations for each near boundary stimulus-choice pair introduced in (B). Markers represent response dilations for each cell and stimulus-choice condition. Boxplots show population medians (horizontal thick lines) and i.q.r. (colored bars). Right: Distribution of stretch in neuronal responses. (**F**) Average population activity from (D) projected onto its first 3 principal components (solid black line), and averages (colored markers) from each stimulus-choice pair projected onto that reference trajectory at stimulus offset for the short near-boundary stimulus (1.38 s). Ghosted versions of these visualizations show their 2D projections onto all possible combinations of PCs 1, 2 and 3. The dashed black arrow indicates the direction of time. (**G**) Average decoded M.A.P. estimates for each stimulus-choice condition. Colored solid lines and patches represent medians and i.q.r. across 512 concatenations (see methods), respectively. (**H**-**L**) Same as (C-G) for the *fixation required* task variant (N = 3 animals, N = 483 neurons).

We trained rats, in both versions of the task, to report intervals of time as either shorter or longer than a 1.5 s category boundary (**Fig. 3A**). Briefly, rats were placed in a rectangular behavioral box with three nose ports positioned at head level (**Fig. 3A**). Trials began with an auditory tone triggered by the subjects' entry into the central "initiation" nose port. After an interval of silence during which subjects were either free to move about the box (no fixation required) (Gouvêa *et al.*, 2015) or required to maintain their snout positioned in the central port (fixation required) (Cruz, Soares and Paton, 2020), a brief second tone was delivered. This second tone acted both as stimulus offset, defining the duration of the interval subjects were asked to judge, and a "go" cue, freeing subjects to report their choice at one of two equidistant ports on either side of the initiation port. Choices reported at one of the lateral noseports following short stimuli (<1.5 s) and at the opposite lateral noseport after long stimuli (>1.5 s) were defined as "correct" and resulted in delivery of a water reward at the choice port. "Incorrect" or premature choices, as well as premature departures from the central port in the fixation version of the task, were punished with an error tone and a time penalty added to the inter-trial-onset interval.

Accuracy of timing judgments (**Fig. 3C**, **H**) and several key features of the recorded striatal population activity in relation to behavior were similar in the two paradigms. First, in both task variants, striatal population state continuously evolved through a set of non-repeating states during interval estimation (**Fig. 3D**, **I**). Furthermore, the time-course of this evolution was systematically related to animal's judgments, a relationship we examined using several approaches that facilitated comparison with the effect of temperature on neural activity described above.

If trial to trial variability in the time-course of neural responses underlies variability in judgments, conditioning trials of a given interval on animals' judgments should result in distributions of neural population speeds with systematically different temporal scaling (**Fig. 3B**). To test this prediction, we focused on intervals where long and short judgments were most balanced, corresponding to the two intervals nearest to 1.5 s. Because rats correctly categorized the majority of trials, even for these "difficult" stimuli, we expect the majority of any hypothetical distribution of population speeds across trials to result in population states at interval offset that lie on the "correct" side of the animal's internal representation of the decision boundary. Thus, conditioning neural data on whether the animal judged 1.38 s as "long" or "short" should create two distributions of trials with respect to population speed: one with an average speed that is slightly slower than the overall average in the case of correct, "short" judgments (**Fig. 3B**, **right panel**, **top left**), and another with an average that is shifted to an even larger extent above the overall average toward faster speeds in the case of incorrect, "long" judgments (**Fig. 3B**, **right panel**, **top right**). Conversely, conditioning neural data on judgment of the 1.62 s interval should create one distribution of trials with an average
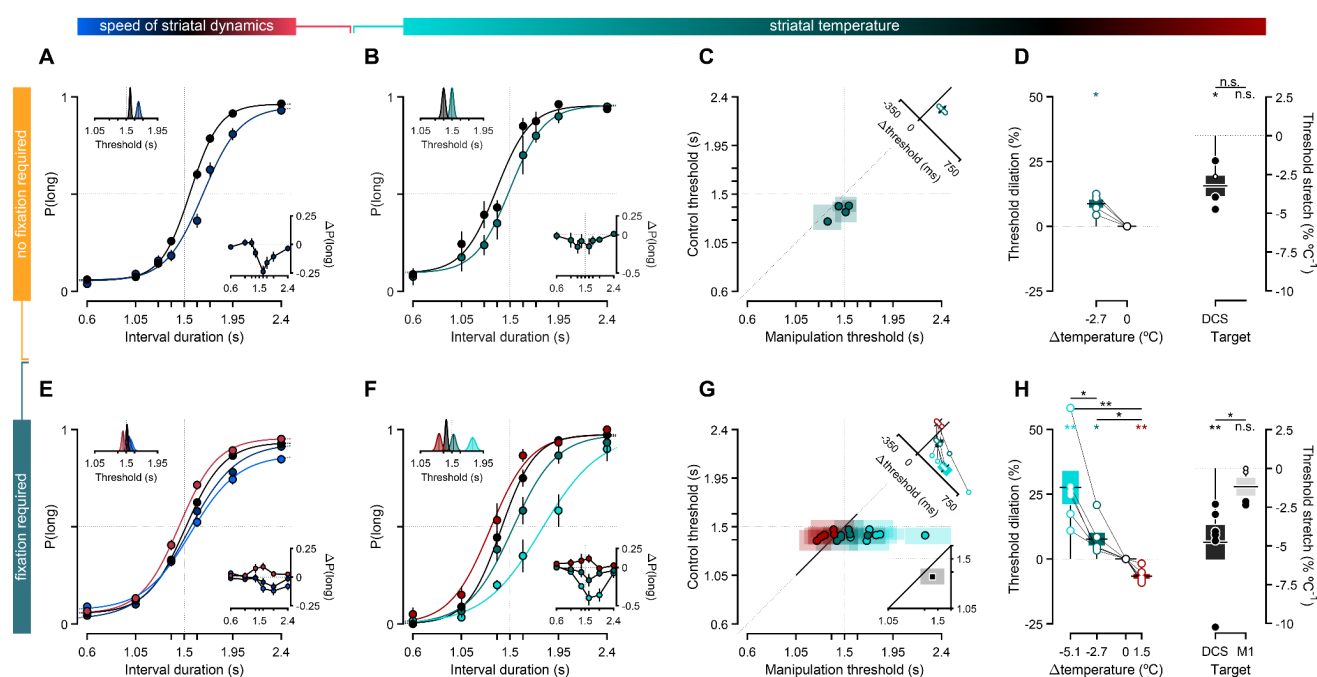
Figure 4. Conditioning behavior on population speed or temperature produced parametric modulation of temporal judgments. (**A**) Performance in the *no fixation* required version of the interval discrimination task conditioned on neural population speed (N = 3). Main axes: psychometric curves split by whether activity progressed more slowly (teal) or at a typical speed (black, see methods). Bottom-right inset: Average differences in proportion of long choices from the slow speed condition to the typical speed condition (mean ± propagated s.e.m.). Top-left inset: Marginal posterior distributions of the threshold parameter for each speed condition's psychometric fit. Solid black lines represent the maximum a posteriori (M.A.P.) point estimates. (**B**) Average performance in the *no fixation* required version of the interval discrimination task conditioned on striatal temperature (N = 4). Main axes: psychometric functions fit to cross-animal average of temperature-split psychophysical data, respectively shown as solid lines and markers of matching color (mean ± s.e.m.). Bottom-right inset: Average differences in proportion of long choices from the manipulation condition to control (mean ± propagated s.e.m.). Top-left inset: Marginal posterior distributions of the threshold parameter for each condition's psychometric fit. Solid black lines represent the maximum a posteriori (M.A.P.) point estimates. (**C**) Main axes: Markers represent M.A.P. estimates and transparent patches the corresponding 95% confidence intervals of threshold parameters fit to individual animals' performance on control (y axis) versus manipulation blocks (x axis). Single animals contribute one data point of each color. Top-right inset: Distribution of threshold differences between manipulation and control condition. Markers represent individual animal differences, bars and error bars are animal means and s.e.m. (**D**) Overall effect of striatal temperature manipulations on psychophysical threshold. Left: Distributions of threshold dilation as a function of induced temperature changes. Markers represent individual animal threshold dilations, linked within animals by thin solid black lines. Right: Distribution of threshold stretch. Markers represent individual animals, and their size and color denote bootstrapped significance. (**E**) Same as in (A), but for the *fixation required* task version and binning neural speed into 4 groups: 2 slower, 1 typical and 1 faster. (**F**-**H**) Same as in (B-D) but for the *fixation required* version of the task (N = 6) and using 3 temperature manipulation doses. (**G**) Bottom-right inset: Same as main axes, but with data from a pilot experiment in which we used a single cooling dose (N = 1). (**H**) Right: Same as in (D), but splitting stretch distributions by manipulation target (DS: N = 6; M1: N = 4).

speed that is slightly *faster* than the overall average in the case of correct, "long" judgments (**Fig. 3B**, **right panel**, **bottom right**), and another with an average that is shifted to an even larger extent *below* the overall average toward slower speeds in the case of incorrect, "short" judgments (**Fig. 3B**,

right panel, **bottom left**). Using the temporal scaling metric applied to recordings under anesthesia above, we found that response dilation of individual neurons systematically varied in accordance with these predictions (**Fig. 3E**, **J**). As with manipulation of temperature, this led to systematic differences in the speed with which population state advanced along its typical trajectory in neural state space (**Fig. 3F**, **K**), and systematic differences in the speed of decoded time estimates derived from the population (**Fig. 3G**, **L**). Lastly, to gain a sense of how population speed might affect choices across a broader range of stimuli, instead of conditioning neural activity on behavior, we conditioned behavior on the speed with which neural population activity evolved along its typical trajectory during the interval period in the two tasks. In both behavioral scenarios, rats were systematically biased toward making "short" judgments the more slowly the population state progressed on single trials, particularly for stimuli closer to the 1.5 s decision boundary, leading to a monotonic relationship between population speed and psychometric *threshold* (**Fig. 4A**, **E**). Thus, variability in timing judgments was associated with the same features of neural activity that were modified by temperature in the first set of experiments. Furthermore, this was true whether or not subjects were required to maintain their position in the initiation port during the interval stimuli, suggesting that decision-related variability in the time course of striatal responses did not result from encoding of kinematic information alone. Next, having established that temperature provides a means of manipulating decision-related variability in striatal activity, we tested whether and how striatal temperature systematically modified subjects' decisions, movement parameters, or both.

### *Striatal temperature systematically modified temporal judgments*

Rats previously trained in either the version of the interval discrimination task not requiring fixation (N = 4) or requiring fixation (N = 6) were implanted with a TED targeting the probe tips to DS (**Fig. 1A**, **Fig. S2E**).

In advance of temperature manipulations, and for both task variants, rats' performance was virtually perfect for easy stimuli, progressively more variable as stimuli approached the categorical boundary and was well described by a sigmoid psychometric function with a threshold close to the experimentally imposed decision boundary of 1.5 s (**Fig. S4**). Strikingly, at the onset of temperature manipulations, all ten subjects across the two task versions displayed a systematic shift towards short judgments when the striatum was cooled (**Fig. 4B**-**D**, **F**-**H**). Furthermore, subjects performing the fixation version of the task exhibited bidirectional and monotonic changes in their discrimination behavior as a function of temperature: rats were more likely to report short judgments during cooling blocks, and more likely to report long judgments during warm blocks, particularly for intervals nearer to the 1.5 s categorical boundary (**Fig. 4F**-**H**). Importantly, the larger the magnitude of the cooling manipulation, the larger the change in choice behavior. The systematic changes in the subjects' judgments caused by temperature were most reliably captured by shifts in the *threshold* parameter of the psychometric curve (**Fig. 4B**, **F top left inset**) - the stimulus duration at which the sigmoid crosses 50% probability of the animal making either a long or short choice. Thresholds tracked differences between control and manipulation temperatures in both sign and magnitude for all individual animals (**Fig. 4C**, **G**). Additionally, the circuit mechanism underlying the behavioral effects of temperature did not seem to involve overlying primary motor cortex (M1), through which the insulated portion of the probes passed, because direct manipulation of M1 temperature in an additional set of four rats produced significantly smaller effects on choice behavior (**Fig. 4H**, **right panel**; **Fig. S2E,S5**), consistent with volume conduction of cortical temperature manipulations to the striatum (**Fig. S1**). Thus, striatal temperature manipulations, shown above to produce changes in the

population response that mimic decision-related temporal scaling of firing patterns, caused highly reproducible, parametric variation in a decision variable used by rats to guide duration judgments during the task. As in the recordings, this effect was robust to differences in task design with respect to the degree that animals were free to move during interval presentation. We thus conclude that the systematic changes in timing judgments induced by temperature in the striatum are due to the effect of temperature on the temporal scaling of neuronal responses within populations of neurons that contribute to the decision.

Striatal temperature did not similarly modify temporal judgments and movement kinematics

What can these results tell us about the nature of the functional involvement of striatal circuits in behavior? One of the most commonly observed effects of dysfunction in BG circuits is a change in the speed of movement, such as bradykinesia in the case of Parkinson's disease. Indeed, inhibiting direct pathway striatal projection neurons has been shown to slow movement without affecting other aspects of its execution (Panigrahi *et al.*, 2015; Cruz, Soares and Paton, 2020). However, the electrophysiological recordings described above demonstrate that temperature monotonically affected population speed, but not firing rate, in the striatum. We thus wondered whether population speed was specifically involved with the temporal evolution of the decision, or additionally involved in regulating movement kinematics. Focusing on the fixation version of the task, we first tracked the position of the TED implant in video using a markerless tracking algorithm (Mathis *et al.*, 2018). We then asked how temperature affected position over time either during the interval period (**Fig. S6A**-**C**), or during choice movements (**Fig. 5A**-**C**).
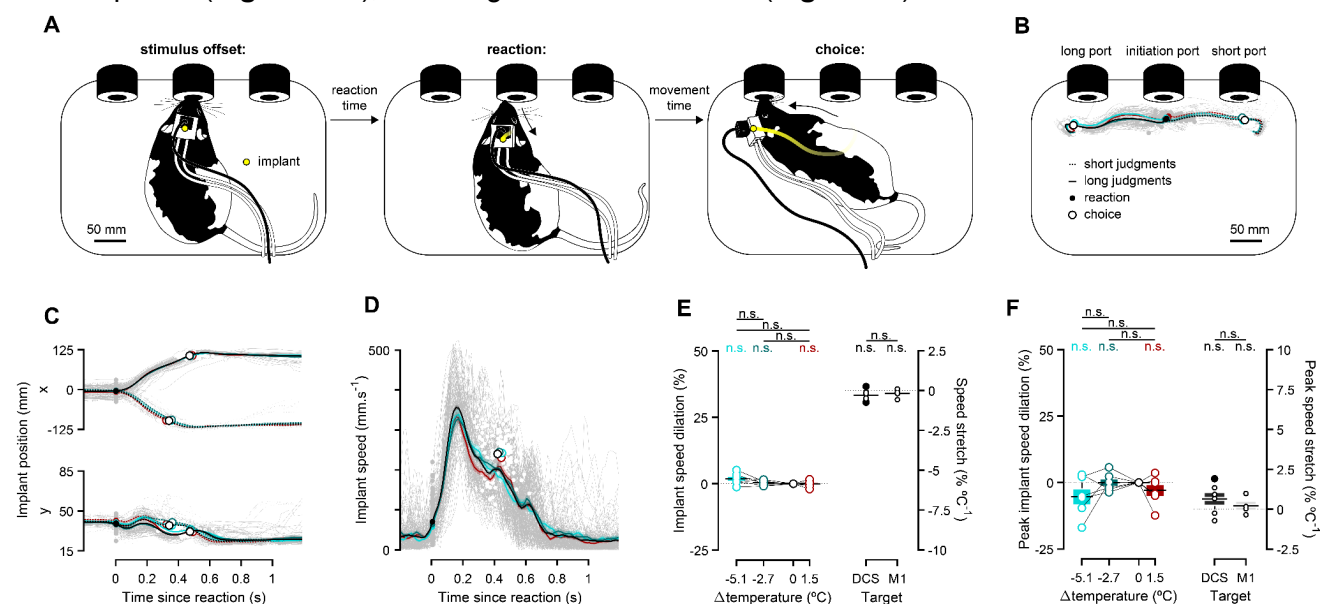
Figure 5. Temperature did not affect the kinematics of movement. (**A**) Illustration of 3 task epochs: stimulus offset (left), reaction (middle) and choice (right). (**B**) 2D trajectories of implant position aligned to reaction from a representative example animal. Dashed (solid) lines correspond to short (long) choices with individual control trials ghosted in the background, and condition-split averages on top. Filled and open markers show position at reaction and choice, respectively. (**C**) Same as in (**B**), split into horizontal (top) and vertical (bottom) coordinates. (**D**) Same data as in (**C**), combined into an overall speed metric. (**E**) Implant speed dilation for DS animals (left) and stretch for DS and M1 animals (right). (**F**) Same as in (**E**) for peak implant speed dilation and stretch. Color scheme indicates temperature as in previous figures.

We did not observe any significant effect of temperature in any case. Rats were positioned similarly during the interval period, and followed similar paths from the fixation port to the choice ports across the different temperatures. In addition, rats moved with indistinguishable velocity profiles to execute their choices (**Fig. 5D,E**). We did observe a slight trend in peak movement velocities as a function of temperature (**Fig. 5F**), but this trend was, if anything, non-monotonic, in striking contrast to the clearly monotonic effect of temperature on decisions and temporal scaling of population activity. Next we analyzed animals' time to react to the interval go cue, and the time taken to move to the choice port. We did not observe significant differences in either reaction times or movement times depending on temperature across rats (**Fig. S6D**-**I**), however, we again observed a trend wherein both warming and cooling appeared to slow movement (**Fig. 5F**, **Fig. S6C**, **F**, **I**, **J**), similar to the trend observed in peak velocity, and similar to the effect that temperature had on the baseline firing rates of recorded striatal neurons (**Fig. 2C**). These observations suggest that the temporal evolution of striatal population state controls the time course of decision variables used by the rats to determine *when* to do *what* action, but that it is not what determines the lower level timing of movement execution. Instead, we find evidence, consistent with published data, that the striatum may provide a lower dimensional gain signal coded in the firing rate of neurons that controls overall vigor (Turner and Desmurget, 2010).

DISCUSSION

Previous work has demonstrated that the speed of neural population activity along reproducible trajectories in neural space can correlate with variability in the timing of actions (Crowe *et al.*, 2014; Murakami *et al.*, 2014; Wang *et al.,* 2017; Remington *et al.*, 2018) and in time-dependent decisions (Leon and Shadlen, 2003; Kim *et al.*, 2013; Gouvêa *et al.*, 2015). Here we show that experimental temperature manipulations in the striatum can be used to slow down or speed up both patterns of neural activity and the temporal evolution of latent decision variables that rats use to guide judgments of duration, and were not explained as a temperature-dependent modulation of movement kinematics. It has long been appreciated in fields as diverse as neuroscience, robotics, and artificial intelligence that control of movement is likely facilitated by a hierarchy of control mechanisms (Krakauer *et al.*, 2019; Merel, Botvinick and Wayne, 2019). The observation that manipulating striatal population speed differentially impacts evolution of decision variables and those required for the timing of movement is consistent with the proposal that the BG act as a mid-level controller of movement, important for selecting among (Doya, 1999), linking (Graybiel, 1998), or modulating (Park, Coddington and Dudman, 2020) different actions but not involved in the details of their execution. Indeed, lesioning dorso-lateral striatum in a motor timing task that involves timed transitions between elements of a motor sequence renders rats unable to perform the sequence (Dhawale *et al.*, 2021). Observations that kinematic information can be decoded from the striatum during tasks that involve timing (Rueda-Orozco and Robbe, 2015; Dhawale *et al.*, 2021) are consistent with this view as well, because BG circuits likely require access to continuous information about the state of sensors and commands being sent to effector systems to determine when to produce particular actions, even if they are not responsible for sending such continuous information for kinematic control to downstream circuits. Such a hierarchical view is reminiscent of the observation that cooling an orofacial region of motor cortex in singing mice slows certain aspects of the song timing while leaving others unchanged (Okobi *et al.*, 2019). Interestingly, tonic inhibition of the direct feedforward pathway of the BG at its initiation point in the striatum can produce a slowing of movement (Panigrahi *et al.*, 2015; Cruz, Soares and Paton, 2020), suggesting that the influence of the BG on control of parameters such as movement speed is not through

11

dynamics in the higher dimensional space of population firing, but rather through a low dimensional, gain-like, modulation of motor programs that are largely implemented by circuitry elsewhere. Consistent with this we found that the non-monotonic effect of striatal temperature on baseline firing rates (**Fig. 2C**), resembled a trend in rats' behavior, which in our dataset did not reach significance, for both warmer and cooler temperatures to slow the peak velocity of choice movements (**Fig. 5F**).

While the effects of temperature on timing judgments were robust in the first sessions of manipulations (**Fig. 4**), these effects diminished with experience (**Fig. S7A,D**). Though we had sought to minimize opportunities for animals to learn to adapt to the temperature manipulations by applying them in blocks of trials lasting only three minutes, always interspersed with a control temperature block (**Fig. 1E**), and alternating manipulation sessions with "washout" sessions where temperature was not manipulated (**Fig. S4C**), we wondered whether animals might have learned to adapt to the effects of temperature. To assess this possibility, we performed a set of behavioral experiments in which the boundary between intervals rewarded for short judgments, and those rewarded for long judgments was shifted in the same blockwise manner (**Fig. S7B**) as was temperature during the previously described experiments. This manipulation was devised to create a similar scenario to that created by striatal temperature manipulations in terms of unsignalled and surprising feedback that could be used by the animal to adapt their decision-making strategy to maximise rewards. Indeed, animals developed the ability to shift their decision thresholds over a small number of sessions, similar to the observed diminishing effects of temperature on temporal judgments (**Fig. S7**). Thus, while temperature manipulations might also produce physiological adaptations that render neural systems more robust to future temperature variations (Robertson and Money, 2012), we found that the changing impact of temperature on timing judgments was consistent with learning to compensate for decision variables whose features might be changing. These data suggest that in general the behavioral impact of manipulating neural systems should be evaluated continuously from the moment the manipulations begin, as opposed to evaluating end-point or average effects alone, as the adaptation ability of animals may be capable of overcoming what are initially significant effects on performance (Fetsch *et al.*, 2018).

During behavior, animals continuously interact with the environment, and this interaction drives significant amounts of neural activity across many brain areas. Pinpointing features of neural activity that underlie latent processes, such as aspects of cognition, in the face of behavior-driven neural activity is a difficult problem requiring multiple approaches. One approach involves studying neural activity across behavioral tasks that vary along dimensions that are orthogonal to the process of interest. For example, signals related to a decision and not its report should be invariant to movement conditions of the task (Parker and Newsome, 1998). In the current study, we found that variability in the speed of striatal population responses correlated with subjects' temporal judgments across two task variants that differed in the degree that subjects were free to move about during stimulus presentation. *A priori*, it is impossible to determine whether such correlations reflect a causal relationship from that neural activity to behavior, an unobserved source of neural activity elsewhere that directly causes both striatal neural activity and behavior, or potentially behavior that causes striatal neural activity through reentrant sensory input. Previous analysis of high speed video during the non-fixation version of the temporal judgment task we study here demonstrated that decision-related information appeared in striatal activity several hundred milliseconds before it appeared in outward behavior, arguing against decision signals being driven by the sensory consequences of behavior alone (Gouvêa *et al.*, 2015). Nonetheless, the existence of such varied possibilities underlies the need for so-called causal manipulations to help determine whether neural

activity is a cause, corollary or a consequence of behavior. Thus, to characterize the impact of temperature on neural activity, we sought to remove behavioral sources of neural variability altogether by focusing on population dynamics elicited by optogenetic activation of VB thalamus under anesthesia. Importantly, in these experiments we did not seek to recapitulate the exact circuit mechanism by which population dynamics are produced during timing behavior. However, VB does integrate somatosensory signals that originate in areas throughout the body, including whisker and orofacial regions. These regions would receive mechanical stimulation at interval onset when rats insert their snout into the initiation port, and thus, VB thalamus represents one potential source of information about the onset of interval stimuli.

What circuit mechanisms might give rise to task-relevant striatal population activity studied here? Previous views have suggested that the BG largely inherit their patterns of activity from inputs, often hypothesized to originate in cortex (Matell and Meck, 2004; Wang *et al.*, 2017; Mikhael and Gershman, 2019). However, if time varying striatal activity underlying temporal judgment were simply inherited from some other brain area, striatal temperature manipulations would be expected to produce a minimal shift and not significant rescaling of behavior (Long and Fee, 2008). As in the vocal control circuit of songbirds, our data thus appear to be inconsistent with a mechanism where the relevant dynamics are simply inherited by the brain area targeted for temperature manipulations, in our case the dorsal striatum. In songbirds, there is evidence that a combination of local circuit mechanisms in pallial area HVC (Egger *et al.*, 2020) and a larger re-entrant circuit involving HVC and multiple other brain areas are involved in generating the temporally patterned activity underlying song timing (Long and Fee, 2008; Hamaguchi, Tanaka and Mooney, 2016). A similar scenario may underlie the mechanisms for generating temporally patterned striatal activity involved in temporal judgments. First, while most network modelling efforts that use neural dynamics for computation have relied at least in part on recurrent excitation, recent work suggests that it may be possible for a largely inhibitory, striatum-like circuit to produce complex spatio-temporal dynamics given sustained excitatory input (Murray and Escola, 2017). The striatum may also represent one stage in a larger re-entrant circuit involving multiple brain systems, where the larger circuit contributes to generation of dynamic patterns of activity that govern the evolution of decision variables. In this view, delays or advances induced by cooling or warming would accumulate with each cycle through the re-entrant circuit, resulting in temporal rescaling with temperature. Such a circuit could in principle involve cortex, BG structures and thalamus (Alexander, Crutcher and DeLong, 1990), or subcortical areas such as downstream BG structures, superior colliculus and thalamus (McHaffie *et al.*, 2005). However, our data suggest that any re-entrant circuit mechanism involving cortex does not include motor cortex, as temperature manipulations there had minimal effects on choice behavior, consistent with previous studies demonstrating that manipulating motor cortex does not affect expert behavior in motor timing tasks (Xu *et al.*, 2014; Kawai *et al.*, 2015). However, orbito-frontal and medial frontal cortical areas have been shown to encode temporal information during both motor timing and temporal judgment tasks, albeit less accurately than in striatum (Kim *et al.*, 2013; Bakhurin *et al.*, 2017), and cooling of medial frontal cortical structures has been shown to delay movements (Xu *et al.*, 2014), potentially indicating involvement of frontal cortical structures. In addition, the activity of midbrain dopamine neurons correlates with and can directly cause changes in timing judgments (Soares, Atallah and Paton, 2016), suggesting that dopaminergic neuromodulation may additionally tune the time-course of network activity through its action on striatal circuits.

Almost a century ago, observations that core body temperature could influence time reproduction and estimation led to the hypothesis that timing was mediated by a "chemical clock" (François, 1927; Hoagland, 1933). Heating or cooling the chemical reactions composing the clock

was proposed to speed or slow them respectively, leading to a faster or more sluggish timekeeping. These ideas later gave way to information processing views of timing that involved a central pacemaker that emits pulses that are accumulated by a counter to estimate passage of time and stored in memory for later use (Treisman, 1963; Gibbon, 1977). More recently, it has been proposed that timing processes are more distributed in the brain, and that networks of neurons possess a rich capacity to act as timekeeping mechanisms through the time-varying patterns of activity they tend to produce, sometimes termed a "population clock". While the data presented here would seem to strongly support this latter hypothesis, in principle the kinds of computations performed by earlier more algorithmic, information processing accounts of timing might well be embedded in the kind of population activity we describe here. This possibility is reflected in a growing belief that the brain performs many of its computations through dynamics (Vyas *et al.*, 2020).

Our percepts, thoughts, and actions are continuously intertwined and regulated in time, and indeed understanding the neural basis of temporal processing has been argued to be a necessary prerequisite for general models of cognition (Finnerty *et al.*, 2015). Yet understanding how the brain appropriately orders and spaces information along the temporal dimension to encode signals that are functions of time has been an enduring challenge for neuroscience. Here we demonstrate that the time-course of activity in populations of striatal neurons directly influences the time-course of a latent timing process used to guide decision-making. The data not only provide a causal link between temporal scaling of a population response and a temporal basis for computation in the brain, but demonstrate that cognitive and motor function can, at least under some circumstances, be dissociated at the level of BG circuits. In the hierarchy of behavioral control, striatal dynamics appear to act at an interface between cognition and motor function to help guide *whether* and *when* to produce particular actions, but not the details of movement execution. Understanding the precise circuit mechanisms responsible for establishing and modulating the timescale of neural activity in these circuits, and which specific computations this activity subserves, represent important future directions of inquiry if we are to understand how the brain draws on internally computed information to produce adaptive and intelligent behavior.

METHODS

Subjects

A total of 32 adult Long-Evans hooded rats (*Rattus norvegicus*) between the ages of 6 and 24 months were used in this study. 2 rats were used in an acute experiment aimed at characterizing the spatiotemporal profile of our temperature manipulation. Another 4 animals were used for an acute experiment combining electrophysiological recordings, temperature manipulation and optogenetic stimulation. 26 wild-type males were trained in the interval discrimination task (across the *fixation required* and *no fixation required* variants), of which 15 were chronically implanted with a custom TED that allowed for temperature manipulation experiments, 6 were implanted with 32-channel tungsten microwire moveable array bundles (Innovative Neurophysiollogy): 3 unilaterally (previously published data (Gouvêa *et al.*, 2015)) and 3 bilaterally. 5 were used in behavioral manipulation experiments. Prior to surgery, animals were kept in pairs in transparent cages with HEPA (High-Efficiency Particulate Air) filters on a 12-hour light-dark cycle (with lights ON at 8 am), at 21 ºC and relative humidity of 50%. All experimental procedures were performed during the light phase of the cycle. Animals used in behavioral experiments had *ad libitum* access to food and were water-deprived. All experimental procedures were in accordance with the European Union Directive

2010/63/EU and approved by the Champalimaud Foundation Animal Welfare Body (Protocol Number: 2017/013) and the Portuguese Veterinary General Board (Direcção-Geral de Veterinária, project approval 0421/000/000/2018).

Behavioral setup

The behavioral apparatus consisted of a 36 cm tall, 22.5 cm wide, and 35 cm long plastic storage box (TROFAST, Ikea) with three floor-level custom nose ports, a speaker (LS00532, Pro Signal) nearing the top of the opposite wall and a custom-made lid that provided uniform lighting and allowed for overhead video recordings (Flea3 FL3-U3-13S2, Point Grey Research Inc.) through an aperture. Each cylinder-shaped nose port was made up of 3D printed components housing a white light emitting diode (LED), an infrared (IR) emitter-sensor pair that enabled the detection of port entries and exits and the accompanying printed circuit board (PCB) (Champalimaud Foundation Scientific Hardware Platform). Additionally, the two lateral ports (positioned symmetrically around the central one) were each equipped with a metallic spout connected to a 20 mL water syringe via a solenoid valve (LHDA1231215H, Lee Company). All sensors, actuators and peripherals were respectively monitored, controlled and kept in the same temporal reference frame using a custom finite state machine implemented by a microcontroller I/O board (Arduino Mega 2560, Arduino) and an interfacing PCB (Champalimaud Foundation Scientific Hardware Platform). Finally, detected port events and other task-relevant behavioral data were timestamped, serially communicated to a Windows 10 desktop computer and stored as a parseable text file using a custom python script. Video was acquired at 60 FPS with a resolution of 1280 x 960 pixels in 8-bit grayscale using Bonsai (Lopes *et al.*, 2015).

Behavioral training

Leading up to the experimental sessions reported in this paper, animals were first trained in 2 hour-long daily sessions 5 times a week in various "tasks" of increasing complexity. During this stage, which we termed Poking101, rats were progressively introduced to the following rules: (un)lit ports are (un)responsive, meaning that nose-poking into a lit port will cause it to turn off and trigger some task event, whereas doing so at an unlit port is inconsequential; entering a lit lateral port results in a reward delivery of 25 uL of water paired with a brief auditory tone (1750 Hz, 150 ms); entering the central port when it is illuminated initiates a trial and *can* lead to both lateral ports lighting up. This is contingent on the animal's snout continuing to interrupt the IR beam at the center port for the entirety of a "fixation delay" (*fixation required* version), or the animal not making a premature entry at either lateral port during the "stimulus presentation delay" (*no fixation required* version). Whichever the task variant, this imposed delay starts off at 0 s and is adaptively marched up towards 3 s (within and across sessions) and consists of an interval of silence demarcated by two brief auditory tones (7500 Hz, 150 ms). Failure to withhold premature departures from the central port (*fixation* version) or choices (*no fixation* version) causes the current trial to be aborted, eliciting an error tone (150 ms of white noise) and adding a timeout of 15 s to the already ticking 9-s inter-trial-onset interval (ITOI). Once animals were able to reliably maintain fixation at the central port (*fixation* version) or defer choices (*no fixation* version) for 3 s, training on the interval discrimination task began ((Gouvêa *et al.*, 2014, 2015)). In it, instead of waiting for a fixed amount of time and collecting a reward at either lateral port once it elapsed, rats were asked to wait for a variable delay on each trial and to then categorize it as either shorter or longer than a boundary of 1.5 s. "Short"

15

judgments were registered at one of the lateral noseports and "long" judgments at the opposite one. Rewards were contingent on stimulus and judgment categories being the same. When this was not the case, an error tone (150 ms of white noise) was played and a time penalty of 10 s was added to the ITOI. Pairs of stimuli symmetric about the categorical boundary were gradually introduced (from easiest to hardest) into the discrete sampling set that animals experienced, until reaching I = {0.6, 1.05, 1.38, 1.62, 1.95, 2.4} s (*fixation* version) or I = {0.6, 1.05, 1.26, 1.38, 1.62, 1.74, 1.95, 2.4} s (*no fixation* version). A correction-loop procedure was used such that, following 3 incorrect categorizations of any given stimulus, only that stimulus was presented to the animal until its associated error count dropped below 3. This training mechanism was disabled during manipulation sessions. It took ~3 months for rats to reach asymptotic performance.

Thermoelectric Device (TED)

Design

We used a custom-made implantable TED (weighing ~30g) based on the Peltier effect to manipulate temperature in neural tissue. The implant consisted of a heat dissipation module, a thermoelectric cooling (TEC) module (01801-9A30-12CN, Custom Thermoelectrics), a 10kΩ thermistor (9707204, Farnell) and two 15-mm long sharpened silver probes. These were insulated down to, but excluding, the tips with a thin layer of PTFE low density thread seal tape (00686081520745, Gasoila) and polyimide tubing. The main distinguishing factors between the implant's initial prototype (used in the single cooling dose experiment) and its final version (used on the 2 bidirectional manipulation cohorts), were that the former was constructed with a passive aluminum heatsink (ICKS25X25X18,5, Fischer Elektronik) and 0.5-mm thick probes insulated with 1-mm wide polyimide tubing (95820-11, Cole-Parmer), whereas the latter had an actively cooled water block (WBA-1.00-0.49-AL-01, Custom Thermoelectrics) and 1-mm thick probes insulated with 2-mm wide polyimide tubing (95820-13, Cole-Parmer). This was used in tandem with a peristaltic pump (200-SMA-150-050, Williamson), male and female Luer adapters (WZ-45504-00, Cole-Palmer) and the required interfacing tubing (WZ-06407-71, Cole-Palmer), allowing for a continuous flow (~15 mL/min) of room temperature water through the water block's inner chambers. The TEC's upper plate was glued to the bottom of the heatsink using thermal glue (TBS20S, TBS), which was also used to secure the thermistor at the center of this module's lower plate. Finally, the two sharpened silver probes were soldered onto the TEC's lower plate (one on each side of the thermistor) using a mixture of lead (419424, Farnell) and silver solder (SDR-9703-030, Custom Thermoelectrics), at a distance of 5 mm from each other. This inter-probe spacing corresponds to two times the ML stereotaxic coordinate of all our DS-targeted implants. Lastly, an RJ45 (85513-5014, Molex) connector was added on top of the heat sink and a custom 3D-printed spacer was mounted on its bottom, both secured using epoxy resin (2022-1, Araldite).

Closed-loop control

The implant was plugged into a custom-made PCB (developed by the Champalimaud Foundation Scientific Hardware Platform and available upon request) via an ethernet cable. This PCB implemented a proportional-integrative-derivative (PID) controller that was designed to bring the implant's thermistor measurement to any experimenter-defined target temperature (within the TEC's range of operation). Briefly, the thermistor readout was continuously compared to the current

temperature setpoint in order to compute an absolute error term (*proportional* channel), a cumulative error (*integrative* channel) and an instantaneous change in error (*derivative* channel). These three error terms were then linearly combined, with weights set by the resistive and capacitive components of the hardware modules that implemented them, and used to modulate the control current driving the TEC. This negative feedback mechanism was optimized so that the target temperature could be reached with negligible delays, steady-state errors and over/undershoots. The resulting closed loop control allowed for stable, safe and transient temperature manipulations, as it required less user intervention, monitorization and arbitration than open loop alternatives. The PID's setpoint was communicated through a serial communication pin from an additional Arduino Mega 2560 board that implemented the temperature manipulation protocol *per se*, meaning it controlled both when to transition into a new block and which temperature to transition to. All block types lasted for 3 minutes, except for control ones in our single cooling dose experiment, which were twice as long to accommodate slower heat dissipation due to this initial experiment's characteristic passive heatsink. In all cases, block transition times and target temperatures were respectively signalled via a brief digital pulse and an additional serial communication port to the task-implementing Arduino board. Both the PID-implementing PCB and the block-controlling Arduino were connected to a computer running Windows 10, where a LabView-based (National Instruments) graphical user interface (TEC visualizer, Champalimaud Foundation Scientific Hardware Platform) enabled online visualization and saving of digitized thermistor temperature measurements (sampled at 100 Hz). Lastly, to prevent irreversible tissue damage in the eventuality of a partial compromise of the closed loop system leading to its "opening", an additional failsafe mechanism was implemented in the PCB's firmware, ensuring that the TEC was automatically disabled if the registered thermistor temperature ever dipped below 0 ºC or rose above 55 ºC.

Calibration

A calibration curve between different set temperatures at the lower plate of the TEC module and temperature measurements at the tip of the silver probes was derived from an acute preparation with an anesthetized rat. Lower plate temperature was set to each value in $T = \{5, 15, 20, 25, 30, 45\}$ ºC, in blocks of 4 minutes, always preceded and followed by a control block of the same duration ($T = 36$ ºC). Temperature at one of the tips of the implant's probe was measured by a second thermistor glued along the probe axis to the polyimide insulation layer. In a separate acute experiment, we positioned a thermistor probe angled at 30º at different distances to the implant's tip ($D = \{0.3, 0.5, 0.9, 2, 5.75\}$ mm), and for each of them repeated the aforementioned blocked calibration procedure (but with manipulation temperatures drawn from the set $T = \{15, 25, 42, 45\}$ ºC). Lastly, all implants were tested individually post-assembly to ensure their respective TEC modules were functioning steadily and properly calibrated, using the same 4-min block protocol in warmed agarose gel (1.5%), which has similar thermal properties to brain tissue (Kim *et al.*, 2007).

Surgical procedures

Acute temperature measurements and calibration

Rats were anesthetized with 2.0-4.5% isoflurane. Animals' body temperature was continuously monitored and maintained at 35 ºC by a rectal probe connected to a closed-loop heating system (FHC, https://www.fh-co.com). After being anaesthetised and before making the first incision, we

administered dexamethasone (2 mg/Kg), carprofen (5 mg/Kg) and a saline solution of atropine (0.05 mg/Kg) subcutaneously. We stereotaxically targeted the DS unilaterally (+0.84 mm AP, +2.5 mm ML from Bregma (Paxinos and Watson, 2013). Immediately following these procedures, animals were perfused for histological confirmation of the measurements' location.

Viral injections

Following the same procedure for induction and maintenance of anesthesia used for acute temperature measurements and calibration, we stereotaxically targeted the ventrobasal complex (VB) of the thalamus for viral delivery (-2.3 mm AP, ±2.8 mm ML, 6.6 mm DV from Bregma (Paxinos and Watson, 2013)). We injected 300nL of rAAV5-CamKII-hChR2(H134R)-EYFP (titer ~10^12 GC%; University of Pennsylvania Vector Core) using an automated microprocessor controlled microinjection pipette with micropipettes pulled from borosilicate capillaries (Nanoject II, Drummond Scientific). Injections were performed at 0.2 Hz with 2.3 nL injection volumes per pulse. For all injections, the micropipette was kept at the injection site 10 minutes before withdrawal. Craniotomies were then covered with Kwik-Cast (WPI) and the skin was closed with sutures (Vicryl, Ethicon Inc.). Animals were allowed to fully recover on a warming pad and returned to the home cage when fully alert. During the 3 days following surgery, animals were given carprofen (5 mg/Kg, SC).

Acute optogenetic stimulation, extracellular recordings, and temperature manipulation

Following 3-6 weeks for viral expression, 4 rats were anesthetized with two doses of urethane, the first at 0.7 g/Kg of body weight and the second at 0.35 g/Kg 20 minutes after. Additionally, we administered dexamethasone (2 mg/Kg), carprofen (5 mg/Kg) and a saline solution of atropine (0.05 mg/Kg) subcutaneously. Animals were then kept with isoflurane at 0.5-1% until at least 30 minutes before electrophysiological recordings began. Animals' body temperature was continuously monitored and maintained at 35 ºC by a rectal probe connected to a closed-loop heating system (FHC, https://www.fh-co.com) throughout the experiments. We opened a large rectangular craniotomy over the left hemisphere (4 mm AP by 3 mm ML from Bregma (Paxinos and Watson, 2013)), centered in the same target location as the chronic implants. A 300 µm diameter and 0.37NA optic fiber (Doric) was targeted to VB (-2.3 mm AP, ±2.8 mm ML, 6.2 mm DV from Bregma (Paxinos and Watson, 2013)), inserted at a 39º angle and secured with blue light cured self adhesive resin cement (RelyX™ Unicem 2 Self-Adhesive Resin Cement, 3M). A small silver ground wire was inserted under the skull of the opposite hemisphere. A TED similar to the one used for chronic implants (with a single silver probe at a 90º angle relative to the heat sink, to accommodate the geometrical demands of the experimental preparation) was lowered to the same DS target location (+0.84 mm AP, -2.5 mm ML, 4 mm DV from Bregma (Paxinos and Watson, 2013)). This modified device was calibrated and behaved similarly to the ones used for chronic manipulations. Finally, a Neuropixels probe (Phase 3A Option 3, IMEC (Jun *et al.*, 2017)) was placed caudally relative to the temperature probe, and slowly lowered to target (5 to 6.5 mm DV) and allowed to stabilize in the tissue for at least 30 minutes before starting recordings and stimulation protocols. Seldomly, and for longer recording protocols, an additional dose of urethane was necessary to maintain anesthesia (0.2 g/Kg). An 473 nm LED source (Doric) was connected to the implanted optical fiber using a patch cord (400 µm core, 0.48 NA) and set to 3.5-5.5 mW at the end of the fiber and controlled using a dedicated arduino that was also responsible for switching the block temperature identity through a serial communication with the TEC controller. Each stimulation trial consisted of a single train of 5, 1-ms long, pulses at 100 Hz (each train lasting 50 ms in total). Each trial was separated by a period

of 1.5 seconds. Electrophysiological and peripheral synchronization (LED and temperature probe) data were simultaneously acquired using SpikeGLX software (https://billkarsh.github.io/SpikeGLX/) at 30kHz. Local-field potential gain and action potential gain were set at 250 and 500, respectively, and split at 300 Hz. Each block at a specific temperature lasted 3 minutes. Temperature identities were drawn, without replacement, from the available set of 3 temperatures and were always intercalated with a control block. This protocol was repeated twice for a total of 2 blocks for each manipulation condition. Immediately following these procedures, animals were perfused for histological confirmation of the measurements' location.

Chronic TED implants

Rats (N = 15; 5 in the single cooling dose experiment, 6 and 4 in the bidirectional striatal and M1 temperature manipulation experiments, respectively) underwent surgery around 3 months after they started training. During the implantation of the TED rats were anesthetized with 2.0-4.5% isoflurane. Animals' body temperature was continuously monitored and maintained at 35 ºC by a rectal probe connected to a closed-loop heating system (FHC, https://www.fh-co.com). After being anaesthetised and before making the first incision, we administered dexamethasone (2 mg/Kg), carprofen (5 mg/Kg) and a saline solution of atropine (0.05 mg/Kg) subcutaneously. We stereotaxically targeted the DS bilaterally (+0.84 mm AP, ±2.5 mm ML from Bregma (Paxinos and Watson, 2013)). Two craniotomies and durotomies matching the diameter of the silver probes were made. 5 support screws were placed: 1 in the occipital plate, 2 posterior and 2 anterior to the location of the craniotomies. The cranial bone was covered with self-curing dental adhesive resin cement (Super-Bond*,* C&B) to improve adherence to the dental acrylic used to secure the implant. The TED was then slowly lowered perpendicular to the brain surface to a depth of 4 mm from cortical surface. The craniotomies were covered with Kwik-Cast (WPI) and the implant was fitted into place and secured with several layers of dental acrylic (the first of which mixed with gentamicin). The procedure ended with suturing (Vicryl, Ethicon Inc.) the skin anterior and posterior to the implant. Animals were allowed to fully recover on a warming pad and returned to the home cage once fully alert. Animals were then individually housed to minimize implant damage. During the 3 days following surgery, animals were injected once a day with carprofen (5 mg/Kg, SC). Animals were allowed to recover for a week after the surgery with food and water *ad libitum*.

Chronic electrophysiology implants

These procedures followed a protocol similar to the one used for the implantation of the chronic TED implants. For a detailed description, see (Gouvêa *et al.*, 2015).

Temperature manipulation protocol

Following one week of recovery since surgery, all animals were again water deprived and gradually resumed behavioral training. Once they were performing at approximately pre-surgical levels in the interval discrimination task described above, they were subjected to temperature manipulation sessions. These 2-h sessions were divided in 3-minute blocks: control blocks, in which the TED was set to body temperature (~36 ºC), always interleaved with manipulation blocks, in which the TED was set to one of 3 manipulation doses (15, 25 and 42 ºC). Manipulation temperatures were drawn at random and without replacement from the aforementioned set until its exhaustion, at which point the set was replenished and the sampling process resumed. Sessions invariably started and ended

with a control block and animals were not explicitly cued to block transitions. Manipulation sessions were interleaved with washout sessions, in which the TED's controller was disabled, and correction-loop training was reinstated.

Implant placement confirmation

Rats were sacrificed with transcardiac perfusion with phosphate-buffered saline (PBS), followed by 4% (wt/vol) paraformaldehyde (PFA). Following perfusion, brains were left in 4% PFA for 24 h and then moved to a 30% sucrose solution (wt/vol) in PBS for 2 to 3 days. For chronic electrophysiology, single-cooling dose and acute experiments, a vibratome was used to section the brain into 50 μm coronal or 40 μm sagittal slices, respectively. Coronal slices were stained with NISSL and sagittal slices series were alternated with NISSL or immunostained with a primary antibody against GFP (A-6455, Invitrogen) and a secondary antibody conjugated with AlexaFluor 488 (ab150077), and finally, incubated in DAPI. Images were acquired with a stereoscope (Lumar V12, Zeiss) or a slide scanner (Axio Scan Z1, Zeiss). For animals subjected to bidirectional chronic temperature manipulations, a 1 T MR scanner (ICON, Brucker) was used to collect MRI data. A T_2-weighted structural image of the brains was collected using a Rapid Imaging with Refocused Echoes (RARE) pulse sequence. The sequence used had a repetition time of 2800 ms, echo time of 90 ms and a RARE factor of 12. The field of view was set to 28 x 15 x 20 mm^2, the spatial resolution of the images was 150 x 150 x 150 μm^3 or 80 x 80 x 80 μm^3 and a matrix of 187 x 100 x 133 voxels was acquired after 8 averages during a 7-hour scanning.

Data analysis

Unless otherwise stated, all data were analyzed using custom MATLAB 2019b (https://www.mathworks.com) scripts.

Psychophysical data analysis

Preprocessing

Trials with reaction times greater than 1 s, or movement times greater than 3 s were labelled as outliers and excluded from all reported analyses. This resulted in less than 5% of all trials being removed. In order to make balanced comparisons across animals and temperature conditions, data from the initial 2 manipulation sessions of every chronically implanted animal were pooled together chronologically up to the point where there were 10 trials per stimulus for each manipulation condition and 40 trials per stimulus for the control temperature condition. The same pooling procedure was applied in reverse for the last 2 temperature and boundary manipulation sessions.

Psychometric function

We used the *Psignifit (Schütt et al., 2015)* toolbox to fit the following 4-parameter psychometric function to all interval discrimination data:

$$\Psi(x; m, w(\alpha), \lambda, \gamma) = \gamma + (1 - \lambda - \gamma) \times S(x; m, w(\alpha))$$

20

$$S_{logistic}(x; m, w(\alpha)) = \frac{1}{1+exp^{-2ln(1/\alpha-1)\times(x-m)/w}}, \alpha = 0.05$$

In this parameterization, a strictly monotonic sigmoid function S from the stimulus level x onto the unit interval $[0, 1]$, is specified by $m = S^{-1}(0.5)$ and $w = S^{-1}(1 - \alpha) - S^{-1}(\alpha)$, namely the *threshold* and *width* parameters. This is independent of the choice of S, which in our case is the logistic function. The hyper-parameter α, which sets the span of w along the y axis, was set to 0.05. To account for stimulus-independent choices, S is scaled by two additional free parameters, λ and γ, which respectively control the upper and lower asymptotes of the psychometric function Ψ. The λ and γ parameters were fixed across temperatures at values found through fitting the corresponding control temperature data.

Dilation & stretch metrics

We adopted the dilation and stretch definitions from (Long and Fee, 2008). Briefly, *dilation* (D) of any scalar metric x (e.g., threshold M.A.P.), was calculated as the percent difference from unity in the ratio of a given temperature's estimate over that of control.

$$D = (\frac{x_{\Delta T}}{x_{\Delta T=0}} - 1) \times 100$$

Stretch (S) was defined as the slope coefficient in a least squares linear regression using dilation as the response variable and the magnitude of our temperature manipulation (induced temperature differences around the implant's tip) as the sole predictor.

$$D = S \times \Delta T + \epsilon$$

Electrophysiological data analysis

Unless otherwise stated, what follows applies to all three electrophysiology data sets analysed in this paper: acute DS recordings (N = 394 neurons, across 4 animals), chronic DS recordings during the *no fixation required* (N = 441 neurons, across 3 animals), and the *fixation required* (N = 483, across 3 animals) versions of the interval discrimination task. We use the generic terms *condition* to refer to striatal temperature in the acute data set, and to stimulus-choice pairs in the two chronic data sets. The *reference* condition corresponds either to control temperature (acute) or to correct categorizations of the 2.4-s stimulus (chronic). Lastly, trial onset refers to the onset of VB stimulation (acute) or stimulus onset (chronic).

Preprocessing

For the 3 animals we recorded from unilaterally in the DS during performance in the *no fixation required* version of the interval discrimination task, preprocessing was done as described when this data set was first published (Gouvêa *et al.*, 2015). For the remaining animals, we used a semi-automated offline approach to detect and sort recorded action potentials into well-isolated units and clusters of multi-unit activity. Detection, sorting and inference of the relative depth of each unit, were done using KiloSort2 (github.com/MouseLand/Kilosort2), whereas curation of the resulting

clusters was performed using Phy (github.com/cortex-lab/phy). Prior to any of the analyses shown in the main figures, we further selected validated units with an intersectional approach that used firing rate and stability, as well as recording depth in the case of the acutely recorded data. Briefly, in order to survive this selection step, units had to: have a mean firing rate of 0.5 Hz or higher; be "stable" throughout the recording session, which we enforced by discarding units for which the Pearson correlation coefficient between average spike density functions computed with two random non-overlapping permutations of reference trials was lower than a 0.75 threshold; and in the case of the acute recordings, have been recorded at a contact that was later inferred to be in the DS, by comparing its position along the Neuropixels probe to a dip in the distribution of recorded cell depths, likely corresponding to a characteristic silence when transitioning from gray (cortex) to white (corpus callosum) to gray (striatum) matter.

Single neuron responses

Spike density functions were built on a trial-by-trial basis by first counting spike times in 2-ms bins and then convolving the resulting histogram with a causal kernel specified by a gamma distribution with shape and scale parameters of $k = 2$ and $\theta = 75$ ms, respectively. Baseline firing rates in the acute recordings were computed in a 500 ms window preceding VB stimulation. To compute temporal scaling factors for each unit-condition pair, we first upsampled reference spike density functions by a factor of 10 and then warped them in time using 1000 scale factors, linearly spaced in the range [0.625, 1.75]. Both the upsampling and time-warping steps were performed using linear interpolation. Next, we linearly regressed all time-warped templates against the spike density function of each condition and stored the corresponding coefficient of determination (R^2). The scale factor that maximized this template-matching metric, is what we operationally defined as the *temporal scaling factor* for that unit and experimental condition. In the case of control scaling factors, we split data into two random non-overlapping sets of trials and arbitrated which one was used to construct templates and which one was the target. Regarding response dilation and stretch, we used the same definitions from the psychophysical analysis section, except that scaling factors (f) replaced ratios of temperature over control estimates when calculating dilation:

$$D = (f - 1) \times 100$$

Low dimensional representations of population state

We used Principal Component Analysis (PCA) to enable visualization of striatal population trajectories in representative 3-dimensional subspaces. Briefly, we first averaged spike density functions across trials of a given condition and concatenated them into $N \times (T \times K)$ matrices, where N is the number of neurons for that data set, T the number of 2-ms time bins relative to trial onset, and K the number of experimental conditions. After normalizing these data to have zero mean and unit standard deviation along the temporal dimension, we used trial-averages corresponding to the reference condition to find the three orthogonal directions that captured the most variance in the data. Lastly, each condition's trial-averaged data were then projected onto the subspace defined by these principal components.

Psychometric curves split by population state at stimulus offset

This analysis was adapted from its original introduction in (Gouvêa *et al.*, 2015), and was only applied to the two chronic data sets in the current paper. Briefly, for all individual trials in each session with 5 or more simultaneously recorded units, we projected population activity at stimulus offset onto the median trajectory traversed by that striatal ensemble during the entire stimulus presentation period. We then normalized these projections by the length of that median trajectory. In addition to this temporal scaling metric, we computed an outlierness metric as the average point-by-point minimum distance between each trial's trajectory and its session's median trajectory (the 5% most extreme trials in these "outlierness" distributions were removed from all subsequent analyses). After pooling all normalized projections over all sessions and animals, we then partitioned, for each stimulus, the resulting distributions into Q groups. For ease of comparison, Q was chosen to match the number of conditions in the temperature manipulation experiments during behavior in the *no fixation required* ($Q = K = 2$) and the *fixation required* ($Q = K = 4$) variants of the interval discrimination task. Psychometric curves were then fit to trials from each group as described above.

Decoding time from ongoing population activity

We used a naïve Bayes decoder (flat prior) to continuously compute probability distributions over elapsed time using multi-session concatenations of putative striatal population activity aligned to trial onset.

Briefly, we:

1) Discretized time t into B 2-ms bins, such that $b \in [1, B]$ and $t_b \in [0, T]$ms, with $T = 1500$ms for the acute recordings and $T = 2400$ms for the chronic recordings;

2) Fit an encoding model to each neuron $n \in [1, N]$ at each point in true time t_b:

$$p(r_n | t_b)$$

Which we determined empirically by querying cell-specific single-trial spike density functions r_n at the true time interval $[t_b, t_{b+1}]$, and smoothing the resulting rate histograms with a gaussian kernel ($\mu = 0, \sigma = 10$Hz). This was done using a subset of trials making up half of all reference trials;

3) Made conditional independence assumptions about neurons, regardless of whether or not they were simultaneously recorded:

$$p(t_b | R) \propto \prod_{n=1}^{N} p(r_n | t_b)$$

Where $R = (r_1, r_2, ..., r_N)$ is a novel, to-be-decoded instance of concatenated population activity recorded at a known condition and point in true time since trial onset;

4) Used Bayes' rule in creating a decoding model that linearly combined all individual neuron encoding models with a uniform prior over decoded time $p(t_b) = \frac{1}{B}$:

$$p(t_b | R) = \frac{p(t_b) \prod_{n=1}^{N} p(r_n | t_b)}{p(R)}$$

23

Where the probability $p(R)$ for the population vector R to occur does not have to be estimated explicitly, as it indirectly follows from normalizing the posterior distribution $p(t_b \mid R)$ such that it sums to 1 over all possible decoder outcomes, i.e., elapsed time as decoded from striatal ongoing activity.

Once the time-dependence in the responses of striatal cells recorded during a set of training trials is known, this Bayesian approach directly addresses the inverse problem: given the firing rates of the same cells, now recorded during previously unseen test trials, how likely is it for any and all b units of time to have passed.

Continuous behavioral data analysis

Preprocessing

Full session 2-h videos were first cut into 12-s long clips (one per trial) aligned to stimulus onset. Offline tracking of the position of several implant features was performed using DeepLabCut (Mathis *et al.*, 2018). Contiguous low confidence position estimates (likelihood < 0.85) of 6 samples or less were linearly interpolated and tracking time series were subsequently smoothed with a 6-sample median filter. In order to standardize units of distance across animals and sessions, we computed session-wise background frames by taking the median pixel intensities from a random sample of 3000 frames from each session's full video. Next, we arbitrarily picked one background frame from a particular session of a particular animal as a reference, and computed the affine transformations that would best align each session's background frame to that reference. These transforms were then applied to both the horizontal and vertical coordinates of each tracked feature and finally, converted to approximately SI units of distance by exploiting knowledge of the behavioral box's dimensions and assuming no optical distortions.

Implant speed profiles

Instantaneous *speed* (s) was computed by taking the one-step forward difference of each feature's displacement (r) with respect to sampling time (Δt).

$$s = \frac{\Delta r}{\Delta t} = \frac{\sqrt{\Delta x^2 + \Delta y^2}}{\Delta t}$$

To compute speed profile dilation and stretch, we used the same template-matching approach described above for single-neuron responses, but using average condition-split speed across time instead of condition-split spike density functions. Lastly, peak speed dilation and stretch were calculated in the same way as threshold dilation and stretch, with each condition's maximum average speed replacing threshold point estimates.

Statistics

Unless otherwise stated, we used one-sample two-tailed t-tests whenever assessing the statistical significance of shifts in distributions, which we visually afforded with vertical solid black lines connecting the distribution's mean to zero. When examining differences across distributions, we

24

used either two-sample two-tailed t-tests when comparing striatal and motor-cortical stretch distributions, or repeated measures ANOVA followed by post-hoc contrasts with Tukey correction for multiple comparisons when comparing experimental dilation distributions across conditions but within cohorts. We visually afforded these two- and paired-sample tests with horizontal solid black lines connecting the two underlying distributions, offset in y for clarity. In all cases, we denote test outcomes near the respective visual affordance with the following notation: *, p<0.05; **, p<0.01; n.s., not significant. In the case of single animal stretch estimates, we assessed their statistical significance at a 5% level by bootstrapping. Specifically, we computed these point estimates for 1000 random samples per manipulation condition, constructed by sampling equal numbers of trials with replacement from the control condition while preserving stimulus identity. For each iteration, we then performed linear regression on bootstrapped dilations and stored the respective slope coefficient as that iteration's stretch. Bootstrapped significance was consistently denoted by larger dark-filled markers, as opposed to smaller white ones.

REFERENCES

Alexander, G. E., Crutcher, M. D. and DeLong, M. R. (1990) 'Basal ganglia-thalamocortical circuits: parallel substrates for motor, oculomotor, "prefrontal" and "limbic" functions', *Progress in brain research*, 85, pp. 119–146.

Aronov, D. and Fee, M. S. (2011) 'Analyzing the dynamics of brain circuits with temperature: design and implementation of a miniature thermoelectric device', *Journal of neuroscience methods*, 197(1), pp. 32–47.

Bakhurin, K. I. *et al.* (2017) 'Differential Encoding of Time by Prefrontal and Striatal Network Dynamics', *The Journal of neuroscience: the official journal of the Society for Neuroscience*, 37(4), pp. 854–870.

Banerjee, A., Egger, R. and Long, M. A. (2021) 'Using focal cooling to link neural dynamics and behavior', *Neuron*, 109(16), pp. 2508–2518.

Buonomano, D. V. and Merzenich, M. M. (1995) 'Temporal information transformed into a spatial code by a neural network with realistic properties', *Science*, 267(5200), pp. 1028–1030.

Coull, J. T. *et al.* (2004) 'Functional anatomy of the attentional modulation of time estimation', *Science*, 303(5663), pp. 1506–1508.

Coull, J. T., Cheng, R.-K. and Meck, W. H. (2011) 'Neuroanatomical and neurochemical substrates of timing', *Neuropsychopharmacology: official publication of the American College of Neuropsychopharmacology*, 36(1), pp. 3–25.

Crowe, D. A. *et al.* (2014) 'Dynamic representation of the temporal and sequential structure of rhythmic movements in the primate medial premotor cortex', *The Journal of neuroscience: the official journal of the Society for Neuroscience*, 34(36), pp. 11972–11983.

Cruz, B. F., Soares, S. and Paton, J. J. (2020) 'Dorsolateral striatal circuits support broadly opponent aspects of action suppression and production'. doi: 10.1101/2020.06.30.180539.

Daw, N. D., Courville, A. C. and Touretzky, D. S. (2006) 'Representation and timing in theories of the dopamine system', *Neural computation*, 18(7), pp. 1637–1677.

Dhawale, A. K. *et al.* (2021) 'The basal ganglia control the detailed kinematics of learned motor

skills', *Nature neuroscience*, 24(9), pp. 1256–1269.

Doya, K. (1999) 'What are the computations of the cerebellum, the basal ganglia and the cerebral cortex?', *Neural networks: the official journal of the International Neural Network Society*, 12(7), pp. 961–974.

Egger, R. *et al.* (2020) 'Local Axonal Conduction Shapes the Spatiotemporal Properties of Neural Sequences', *Cell*, 183(2), pp. 537–548.e12.

Fetsch, C. R. *et al.* (2018) 'Focal optogenetic suppression in macaque area MT biases direction discrimination and decision confidence, but only transiently', *eLife*, 7. doi: 10.7554/eLife.36523.

Finnerty, G. T. *et al.* (2015) 'Time in Cortical Circuits', *The Journal of neuroscience: the official journal of the Society for Neuroscience*, 35(41), pp. 13912–13916.

François, M. (1927) 'VI. Contribution à l'étude du sens du Temps. La température interne comme facteur de variation de l'appréciation subjective des durées', *L'Année psychologique*, 28(1), pp. 186–204.

Freeman, J. S. *et al.* (1996) 'Abnormalities of motor timing in Huntington's disease', *Parkinsonism & related disorders*, 2(2), pp. 81–93.

Gallistel, C. R. and Gibbon, J. (2000) 'Time, rate, and conditioning', *Psychological review*, 107(2), pp. 289–344.

Gibbon, J. (1977) 'Scalar expectancy theory and Weber's law in animal timing', *Psychological review*, 84(3), p. 279.

Gouvêa, T. S. *et al.* (2014) 'Ongoing behavior predicts perceptual report of interval duration', *Frontiers in neurorobotics*, 8, p. 10.

Gouvêa, T. S. *et al.* (2015) 'Striatal dynamics explain duration judgments', *eLife*, 4. doi: 10.7554/eLife.11386.

Graybiel, A. M. (1998) 'The basal ganglia and chunking of action repertoires', *Neurobiology of learning and memory*, 70(1-2), pp. 119–136.

Hamaguchi, K., Tanaka, M. and Mooney, R. (2016) 'A Distributed Recurrent Network Contributes to Temporally Precise Vocalizations', *Neuron*, 91(3), pp. 680–693.

Hidalgo-Balbuena, A. E. *et al.* (2019) 'Sensory representations in the striatum provide a temporal reference for learning and executing motor habits', *Nature communications*, 10(1), pp. 1–15.

Hoagland, H. (1933) 'The Physiological Control of Judgments of Duration: Evidence for a Chemical Clock', *The Journal of general psychology*, 9(2), pp. 267–287.

Jazayeri, M. and Shadlen, M. N. (2015) 'A Neural Mechanism for Sensing and Reproducing a Time Interval', *Current biology: CB*, 25(20), pp. 2599–2609.

Jin, D. Z., Fujii, N. and Graybiel, A. M. (2009) 'Neural representation of time in cortico-basal ganglia circuits', *Proceedings of the National Academy of Sciences of the United States of America*, 106(45), pp. 19156–19161.

Jun, J. J. *et al.* (2017) 'Fully integrated silicon probes for high-density recording of neural activity',

Nature, 551(7679), pp. 232–236.

Kawai, R. *et al.* (2015) 'Motor cortex is required for learning but not for executing a motor skill', *Neuron*, 86(3), pp. 800–812.

Killeen, P. R. and Fetterman, J. G. (1988) 'A behavioral theory of timing', *Psychological review*, 95(2), pp. 274–295.

Killeen, P. R. and Fetterman, J. G. (1993) 'The behavioral theory of timing: transition analyses', *Journal of the experimental analysis of behavior*, 59(2), pp. 411–422.

Kim, J. *et al.* (2013) 'Neural correlates of interval timing in rodent prefrontal cortex', *The Journal of neuroscience: the official journal of the Society for Neuroscience*, 33(34), pp. 13834–13847.

Kim, J., Kim, D. and Jung, M. W. (2018) 'Distinct Dynamics of Striatal and Prefrontal Neural Activity During Temporal Discrimination', *Frontiers in integrative neuroscience*, 12, p. 34.

Kim, S. *et al.* (2007) 'Thermal impact of an active 3-D microelectrode array implanted in the brain', *IEEE transactions on neural systems and rehabilitation engineering: a publication of the IEEE Engineering in Medicine and Biology Society*, 15(4), pp. 493–501.

Krakauer, J. W. *et al.* (2019) 'Motor Learning', *Comprehensive Physiology*, 9(2), pp. 613–663.

Leon, M. I. and Shadlen, M. N. (2003) 'Representation of time by neurons in the posterior parietal cortex of the macaque', *Neuron*, 38(2), pp. 317–327.

Long, M. A. *et al.* (2016) 'Functional Segregation of Cortical Regions Underlying Speech Timing and Articulation', *Neuron*, 89(6), pp. 1187–1193.

Long, M. A. and Fee, M. S. (2008) 'Using temperature to analyse temporal dynamics in the songbird motor pathway', *Nature*, 456(7219), pp. 189–194.

Lopes, G. *et al.* (2015) 'Bonsai: an event-based framework for processing and controlling data streams', *Frontiers in neuroinformatics*, 9, p. 7.

Machado, A., Malheiro, M. T. and Erlhagen, W. (2009) 'Learning to Time: a perspective', *Journal of the experimental analysis of behavior*, 92(3), pp. 423–458.

Malapani, C. *et al.* (1998) 'Coupled temporal memories in Parkinson's disease: a dopamine-related dysfunction', *Journal of cognitive neuroscience*, 10(3), pp. 316–331.

Matell, M. S. and Meck, W. H. (2004) 'Cortico-striatal circuits and interval timing: coincidence detection of oscillatory processes', *Brain research. Cognitive brain research*, 21(2), pp. 139–170.

Matell, M. S., Meck, W. H. and Nicolelis, M. A. L. (2003) 'Interval timing and the encoding of signal duration by ensembles of cortical and striatal neurons', *Behavioral neuroscience*, 117(4), pp. 760–773.

Mathis, A. *et al.* (2018) 'DeepLabCut: markerless pose estimation of user-defined body parts with deep learning', *Nature neuroscience*, 21(9), pp. 1281–1289.

McHaffie, J. G. *et al.* (2005) 'Subcortical loops through the basal ganglia', *Trends in neurosciences*, 28(8), pp. 401–407.

Meck, W. H. (2006) 'Neuroanatomical localization of an internal clock: a functional link between

mesolimbic, nigrostriatal, and mesocortical dopaminergic systems', *Brain research*, 1109(1), pp. 93–107.

Mello, G. B. M., Soares, S. and Paton, J. J. (2015) 'A scalable population code for time in the striatum', *Current biology: CB*, 25(9), pp. 1113–1122.

Merchant, H. and Averbeck, B. B. (2017) 'The Computational and Neural Basis of Rhythmic Timing in Medial Premotor Cortex', *The Journal of neuroscience: the official journal of the Society for Neuroscience*, 37(17), pp. 4552–4564.

Merel, J., Botvinick, M. and Wayne, G. (2019) 'Hierarchical motor control in mammals and machines', *Nature communications*, 10(1), p. 5489.

Mikhael, J. G. and Gershman, S. J. (2019) 'Adapting the flow of time with dopamine', *Journal of neurophysiology*, 121(5), pp. 1748–1760.

Murakami, M. *et al.* (2014) 'Neural antecedents of self-initiated actions in secondary motor cortex', *Nature neuroscience*, 17(11), pp. 1574–1582.

Murray, J. M. and Escola, G. S. (2017) 'Learning multiple variable-speed sequences in striatum via cortical tutoring', *eLife*, 6. doi: 10.7554/eLife.26084.

Okobi, D. E., Jr *et al.* (2019) 'Motor cortical control of vocal interaction in neotropical singing mice', *Science*, 363(6430), pp. 983–988.

Panigrahi, B. *et al.* (2015) 'Dopamine Is Required for the Neural Representation and Control of Movement Vigor', *Cell*, 162(6), pp. 1418–1430.

Parker, A. J. and Newsome, W. T. (1998) 'Sense and the single neuron: probing the physiology of perception', *Annual review of neuroscience*, 21, pp. 227–277.

Park, J., Coddington, L. T. and Dudman, J. T. (2020) 'Basal Ganglia Circuits for Action Specification', *Annual review of neuroscience*, 43. Available at: https://www.annualreviews.org/doi/abs/10.1146/annurev-neuro-070918-050452.

Paton, J. J. and Buonomano, D. V. (2018) 'The Neural Basis of Timing: Distributed Mechanisms for Diverse Functions', *Neuron*, 98(4), pp. 687–705.

Paxinos, G. and Watson, C. (2013) *The Rat Brain in Stereotaxic Coordinates: Hard Cover Edition*. Academic Press.

Petersen, P. C. and Buzsáki, G. (2020) 'Cooling of Medial Septum Reveals Theta Phase Lag Coordination of Hippocampal Cell Assemblies', *Neuron*, 107(4), pp. 731–744.e3.

Rao, S. M., Mayer, A. R. and Harrington, D. L. (2001) 'The evolution of brain activation during temporal processing', *Nature neuroscience*, 4(3), pp. 317–323.

Remington, E. D. *et al.* (2018) 'Flexible Sensorimotor Computations through Rapid Reconfiguration of Cortical Dynamics', *Neuron*, 98(5), pp. 1005–1019.e5.

Robertson, R. M. and Money, T. G. A. (2012) 'Temperature and neuronal circuit function: compensation, tuning and tolerance', *Current opinion in neurobiology*, 22(4), pp. 724–734.

Rueda-Orozco, P. E. and Robbe, D. (2015) 'The striatum multiplexes contextual and kinematic

information to constrain motor habits execution', *Nature neuroscience*, 18(3), pp. 453–460.

Safaie, M. *et al.* (2020) 'Turning the body into a clock: Accurate timing is facilitated by simple stereotyped interactions with the environment', *Proceedings of the National Academy of Sciences*, 117(23), pp. 13084–13093.

Schütt, H. *et al.* (2015) 'Psignifit 4: Pain-free Bayesian Inference for Psychometric Functions', *Journal of Vision*, p. 474. doi: 10.1167/15.12.474.

Soares, S., Atallah, B. V. and Paton, J. J. (2016) 'Midbrain dopamine neurons control judgment of time', *Science*, 354(6317), pp. 1273–1277.

Tang, L. S. *et al.* (2010) 'Precise Temperature Compensation of Phase in a Rhythmic Motor Pattern', *PLoS Biology*, p. e1000469. doi: 10.1371/journal.pbio.1000469.

Treisman, M. (1963) 'Temporal discrimination and the indifference interval: Implications for a model of the" internal clock"', *Psychological Monographs: General and Applied*, 77(13), p. 1.

Turner, R. S. and Desmurget, M. (2010) 'Basal ganglia contributions to motor control: a vigorous tutor', *Current opinion in neurobiology*, 20(6), pp. 704–716.

Vyas, S. *et al.* (2020) 'Computation Through Neural Population Dynamics', *Annual review of neuroscience*, 43, pp. 249–275.

Wang, J. *et al.* (2017) 'Flexible timing by temporal scaling of cortical responses', *Nature neuroscience*. doi: 10.1038/s41593-017-0028-6.

Xu, M. *et al.* (2014) 'Representation of interval timing by temporally scalable firing patterns in rat prefrontal cortex', *Proceedings of the National Academy of Sciences of the United States of America*, 111(1), pp. 480–485.

ACKNOWLEDGEMENTS

Author contributions: TM, FSR, MP, JJP devised the experiments, TM, FSR, MP performed all experiments, analyzed the data and drafted and edited the manuscript. BFC helped design and perform electrophysiology experiments and reviewed the manuscript. AIG performed a subset of

temperature manipulation experiments during behavior and reviewed the manuscript. PERO devised and assisted in implementing the method of optogenetically stimulating reproducible striatal dynamics and reviewed the manuscript. JJP supervised all aspects of the project and drafted and edited the manuscript.

Competing interests: The authors declare no competing financial interests.

Materials & Correspondence: The data and analysis code that support the findings of this study are available from the corresponding author upon reasonable request.

SUPPLEMENTAL FIGURES
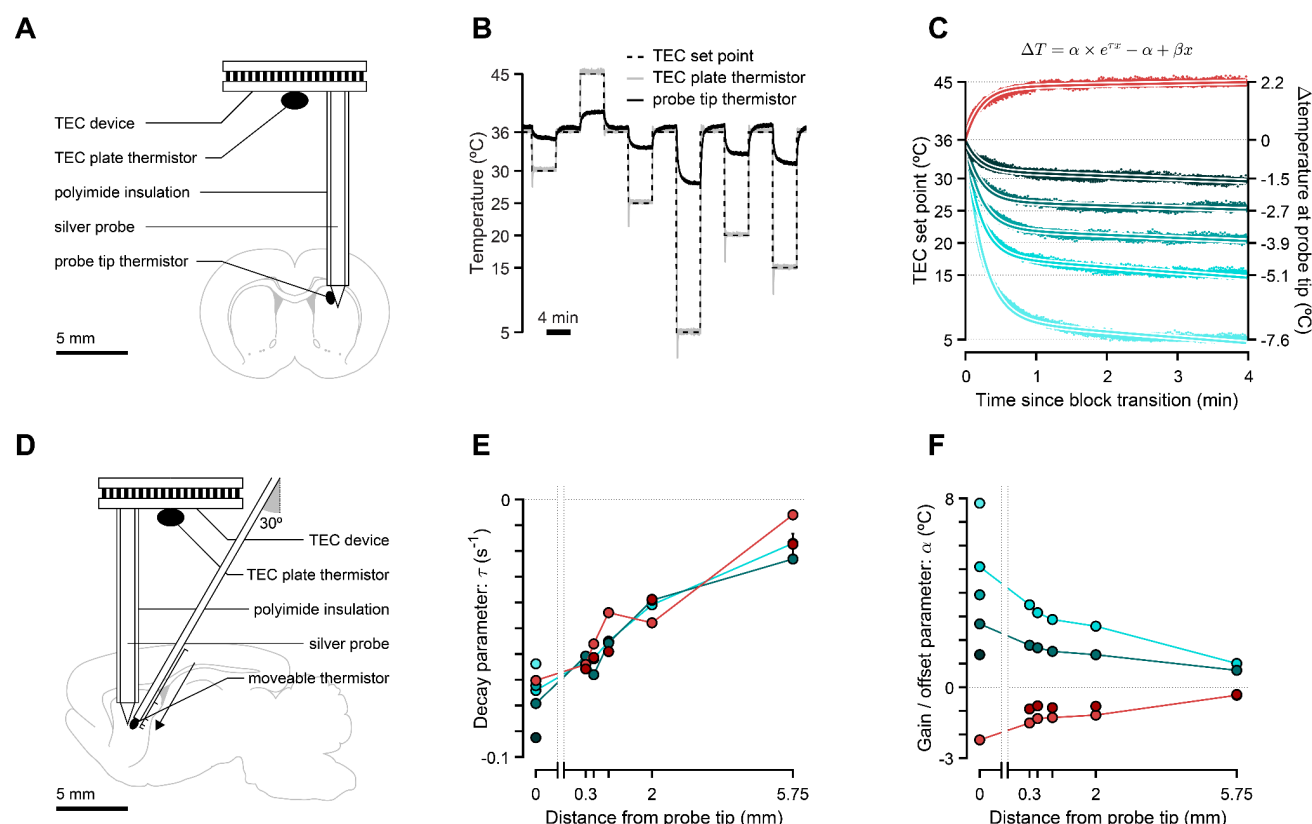
Figure S1. Spatiotemporal characterization of thermoelectric device (TED). (**A**) Schematic of the preparation in which we set our TED to one of several manipulation temperatures (T = {5, 15, 20, 25, 30, 45} ºC) while measuring temperature at its lower plate and probe tip simultaneously. (**B**) Temperature measured at the TEC plate and probe tip thermistors. (**C**) Temperature traces measured at the probe tip thermistor during manipulation blocks aligned to block transitions. Solid lines represent model fits. (**D**) Schematic of the preparation in which we set our TED to one of several manipulation temperatures (T = {15, 25, 42, 45} ºC) while measuring temperature at its lower plate a movable temperature probe simultaneously. (**E**) Decay parameters for models fit to manipulation temperatures (as shown in (C)) across the 2 experiments (manipulation temperatures that are common to both experiments are connected with solid colored lines). (**F**) Same as (E), but for the gain / offset parameter across all model fits.

31
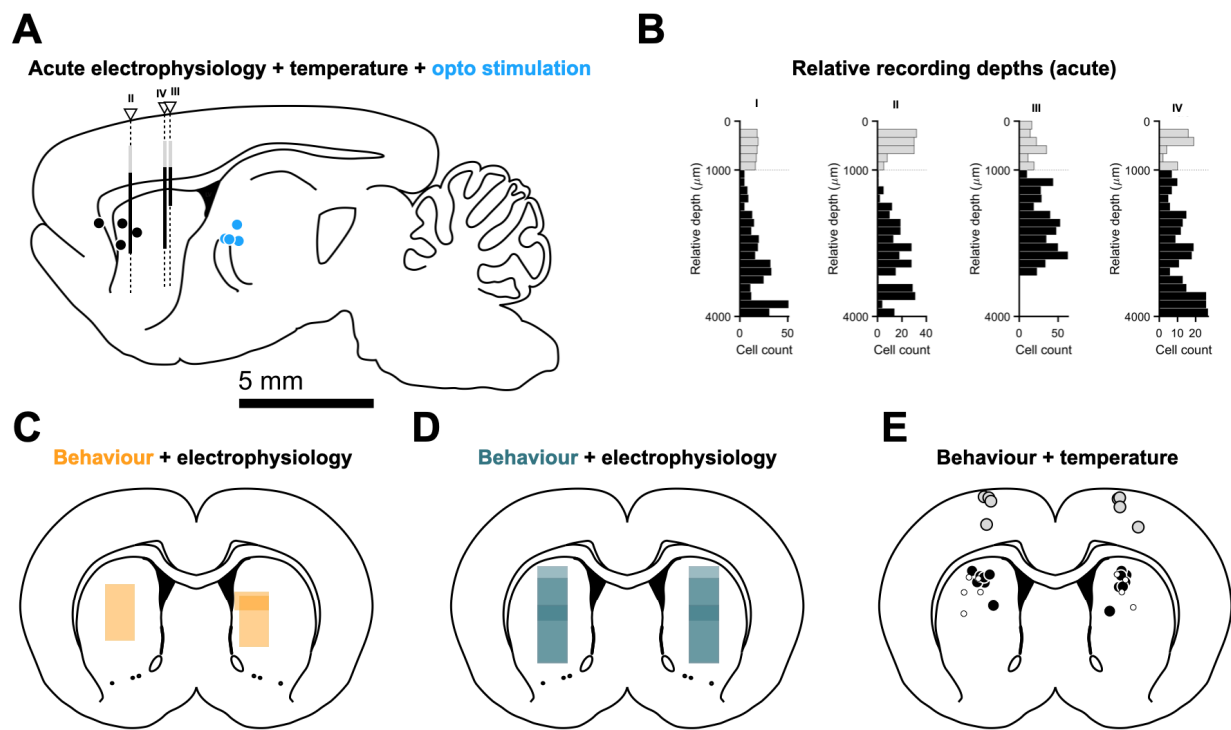
Figure S2. Histological reconstruction of TED, optical fiber and recordings probe placements for acute and chronic experiments. (**A**) Intermediate medial-lateral (ML) locations of TED probes (black markers), optical fibers (blue markers) and Neuropixels probes (white triangles) projected onto a reference sagittal slice (ML = 2.62 mm from Bregma). (**B**) Distributions of relative recording depths for all animals (N = 4) and recorded units (N = 335). Horizontal dashed line represents corpus callosum. Putative motor cortical and striatal neurons in gray and black, respectively. Histograms' relative depth is overlaid in (A) using the same color scheme. We were unable to clearly identify the Neuropixels tract for animal I. (**C**-**E**) Intermediate anterior posterior (AP) location of microwire recording bundles in the *no fixation required* (C, orange, N = 3 animals implanted unilaterally), *fixation required* (D, petrol blue, N = 3 animals implanted bilaterally) and TED (E) probes for striatal (black markers, N = 6) and cortical (gray markers, N = 4) targets projected onto target coronal slice (AP = +0.84 mm from Bregma). White markers show implant locations for the *no fixation required* striatal cooling experiment (N = 5).
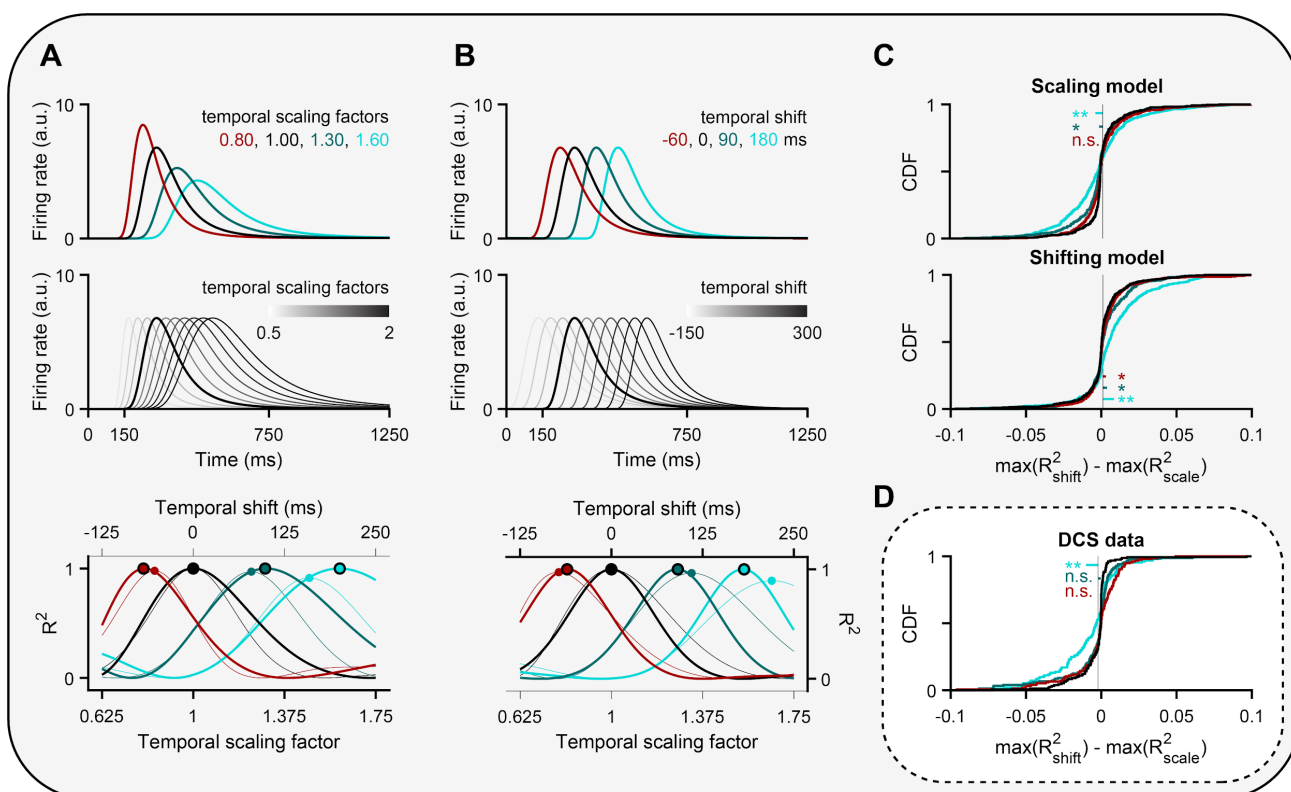
Figure S3. Temporal scaling as opposed to shifting provided a better account of temperature's effect on neural activity. (**A**) Top: Simulated spike density functions exhibiting bidirectional and dose-dependent temporal scaling with temperature. Middle: Templates built by warping a control spike density function (thicker black line) in time by scale factors ranging from 0.625 (maximum contraction) to 1.75 (maximum dilation). Note that when applying this method to data, this control response is not the same as the one shown in the top panel, as the two are built using two non-overlapping random sets of control trials. Bottom: Thick lines represent the coefficient of determination (R^2) for all scaled templates in the middle panel regressed against each of the target spike density functions shown at the top. We computed this objective function for each neuron-temperature condition pair and took its global maximum as the corresponding temporal scaling factor, highlighted here by the larger markers. Thinner lines and smaller markers depict R^2 values for a similar regression procedure applied to a series of shifted, as opposed to scaled, templates (see B). (**B**) Same as (A), except that for artificially temporally shifted responses relative to control (top), temporally shifted templates (middle), and their regression outcomes (bottom). The thinner lines and smaller markers respectively represent the R^2 curves and maxima resulting from regressing the scaled templates from A, middle against the shifted targets in B, top. Conversely, the result of regressing shifted templates against scaled targets is plotted in the same manner in (A, bottom). (**C**) To assess whether the effects of temperature on individual striatal responses were better accounted for by temporal scaling or shifting, we built two separate spiking models in which we either injected one effect or the other. Briefly, we modeled 500 control firing rate functions as gaussian bumps defined over 1.5 s with means spanning the interval from 150 ms to 750 ms (**Fig. 1D**) and a standard deviation of 50 ms. The amplitudes of the resulting probability density functions were rescaled so that their distribution of mean firing rates matched that of striatal data. Next, we created one additional rate function per neuron per manipulation condition by either shifting or scaling its control response in time. Again, the distribution of generative temporal scaling factors and shifts used was informed by the empirical distributions of these metrics extracted from striatal data. We then generated 150 spike trains of each condition per neuron by sampling spike times from inhomogeneous Poisson point processes with the aforementioned condition-specific responses as their time-dependent rate parameters. From this point on, we proceeded to analyze the resulting spike "data" in the exact same way we did for the striatal data, by first averaging trials within condition,

33

generating libraries of templates and then computing temporal scaling factors and shifts. Finally, for each "neuron"-condition pair within each model, we stored the R^2 values corresponding to the best-matching scaled and shifted templates and subtracted the former from the latter to build the distributions shown here at the top (scaling model) and middle (shifting model) panels. Thick solid sigmoidal lines represent the CDFs of each condition's R^2 difference. Thin vertical black lines denote control mean differences. Small horizontal colored lines link the respective means of the corresponding manipulation and control distributions. (**D**) Same as (C), but for striatal data.
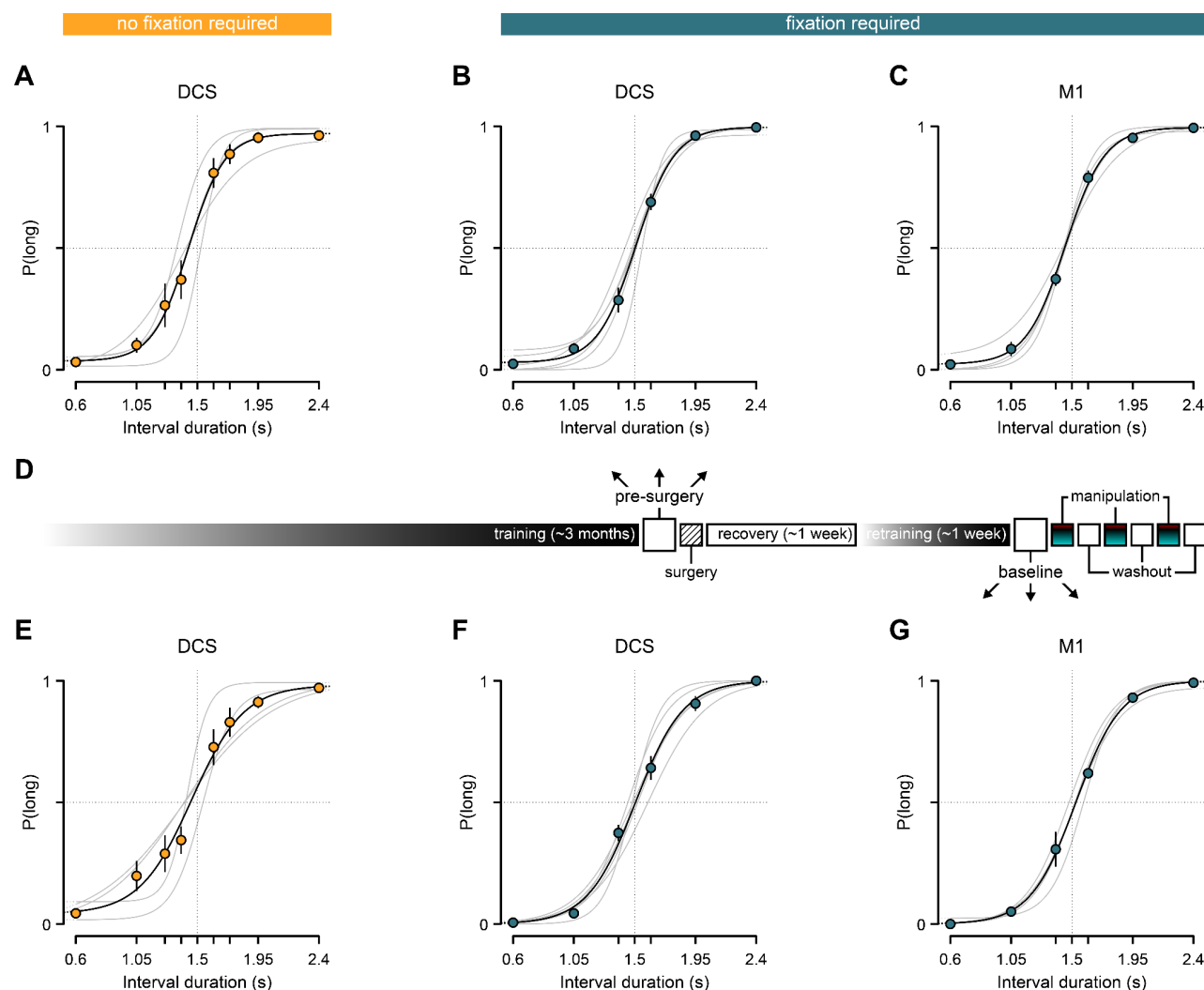
Figure S4. Discrimination performance in both task variants was qualitatively similar before and after TED implantation. (**A**) Discrimination performance of the cohort of rats that were trained on the *no fixation required* variant of the interval discrimination task and eventually implanted with the initial version of our custom TED targeting the DS (N = 4) on the last day of training before surgery. Gray lines are psychometric fits to individual animals. The black one is a fit to the average across animals. So as to prevent visual clutter, the underlying choice data is only shown for the cohort average (mean +- s.e.m.). (**B**) Same as (A), but for the cohort of rats that were trained on the *fixation required* task variant and eventually implanted with the final version of our custom TED targeting the DS (N = 6). (**C**) Same as (B), but for the cohort of rats that were eventually implanted with the final version of our custom TED targeting M1 (N = 4). (**D**) Cartoonized timeline for a typical experimental rat. Elongated bars illustrate long periods of time, whereas squares represent individual daily sessions, which, with the exception of surgeries, lasted for 2 hours. (**E**-**G**) Same as (A-C), but for the last post-surgery training session in advance of starting temperature manipulation sessions.
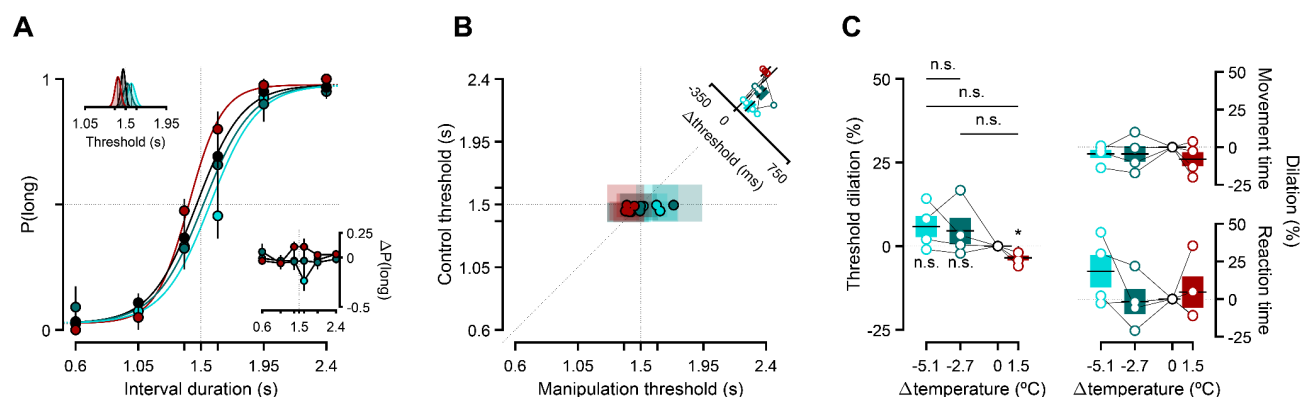
Figure S5. Manipulating the temperature of M1 cortex produced markedly smaller effects on timing judgments. (**A**) Average discrimination performance at the onset of M1 temperature manipulations. Main axes: psychometric functions fit to cross-animal averages (N = 4) of temperature-split psychophysical data, respectively shown as solid lines and markers of matching color (mean ± s.e.m.). Bottom-right inset: Average differences in proportion of long choices from each manipulation condition to control (mean ± propagated s.e.m.). Top-left inset: Marginal posterior distributions of the threshold parameter for each condition's psychometric fit. Solid black lines represent the M.A.P. point estimates implicit in the fits shown in the main axes. (**B**) Animal-split discrimination behavior at the onset of M1 temperature manipulations. Main axes: Markers represent M.A.P. estimates and transparent patches the corresponding 95% confidence intervals of threshold parameters fit to individual animals' performance on control (y axis) versus manipulation blocks (x axis). The identity line is plotted as a diagonal line. Inset: Distribution of threshold differences between manipulation and control conditions. Markers represent individual animal differences, bars and error bars are animal means and s.e.m. (**C**) Effect of motor cortical temperature manipulations on psychophysical threshold (left), reaction (bottom right) and movement times (top right). Markers represent individual metric dilations, linked within animals by thin solid black lines. Boxplots show animal means (horizontal thick black lines) and s.e.m. (colored bars).
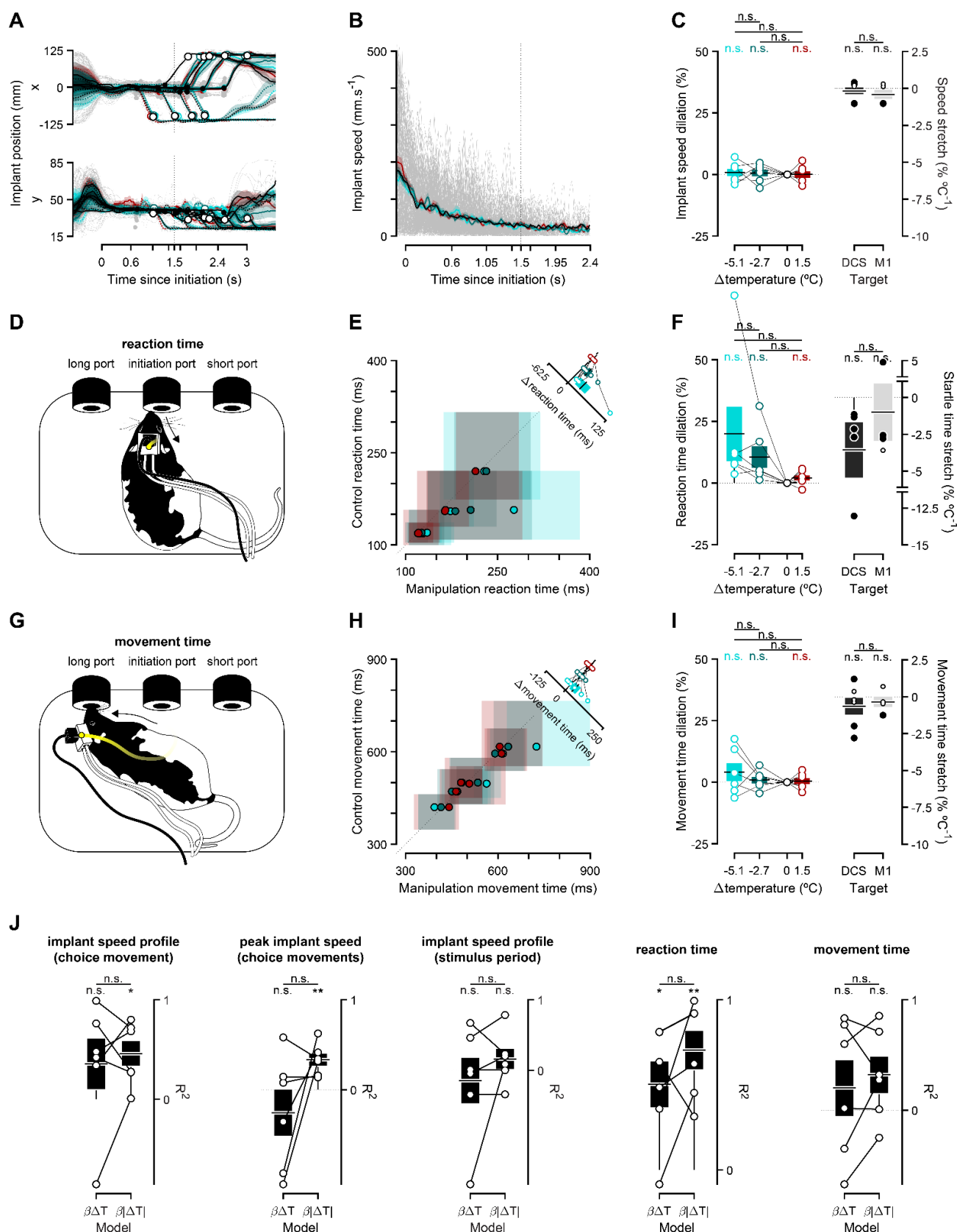
Figure S6. Temperature did not produce monotonic effects on movement during stimulus presentation, latency to initiate, or time to execute choice movements. (**A**) Horizontal (top) and vertical (bottom)

coordinates of implant position aligned to stimulus onset (representative example animal). Dashed (solid) lines correspond to short (long) choices with individual control trials ghosted in the background, and condition-split averages on top. Filled and open markers show position at reaction and choice, respectively. (**B**) Same data as in (A), combined into an overall speed metric. (**C**) Implant speed dilation for DS animals (left) and stretch for DS and M1 animals (right). (**D**) Schematics highlighting the task epoch in between stimulus offset and the initiation of the choice movement (reaction time). (**E**) Main axes: Markers represent the median and transparent patches the corresponding i.q.r. of individual animals' reaction times on control (y axis) versus manipulation blocks (x axis). Single animals contribute one data point of each color. The identity line is plotted as a diagonal line. Its thick solid portion highlights the region of the main axes that is shown in the bottom-right inset axes. Top-right inset: Distribution of reaction time differences between manipulation and control condition. Markers represent individual animal differences, bars and error bars are animal means and s.e.m. (**F**) Left: Distributions of median reaction time dilations as a function of induced temperature changes. Markers represent individual reaction time dilations, linked within animals by thin solid black lines. Right: Distribution of median reaction time stretches. Markers represent individual animals, and their size and color denote bootstrapped significance. (**G-I**) Same as (D-F), but for the task epoch in between the initiation of the choice movement and the moment that choice is registered (movement time). (**J**) Comparison between 2 one-parameter models of how temperature affects all movement-related metric dilations reported. On each panel, the goodness of fit of the monotonic (left) and the non-monotonic (right) model, as measured by its coefficient of determination (R^2), is shown for individual animals (open markers) and the population (mean ± s.e.m.). Note that the coefficient in the monotonic model corresponds to the stretch metric used throughout.
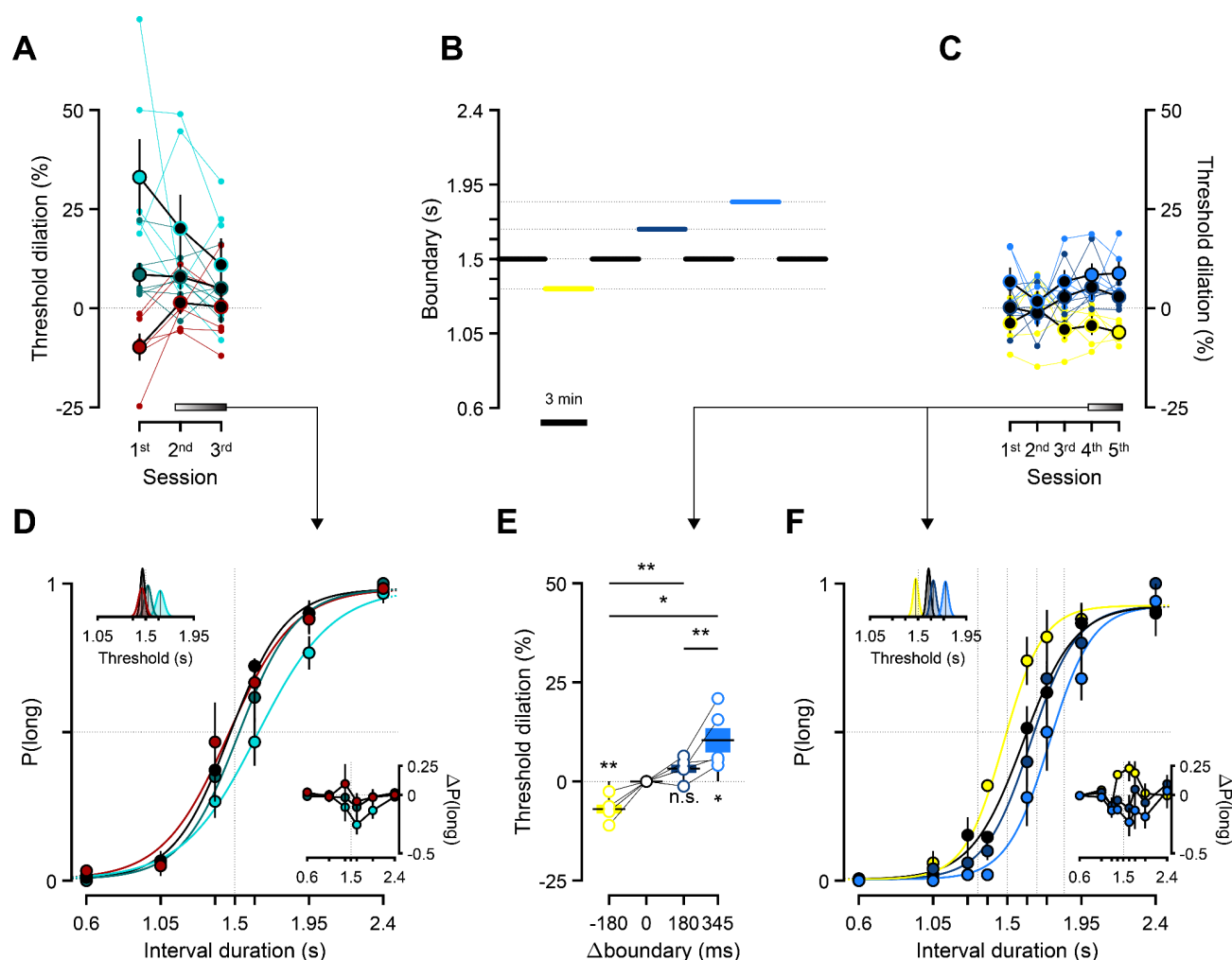
Figure S7. Animals adapted their behavior to both temperature and category boundary manipulations. (**A**) Threshold dilation across the first three temperature manipulation sessions for the striatal cohort shown in **Fig. 2** (N = 6). Small markers and thin lines linking them refer to threshold dilations for individual animals. Larger markers correspond to cross-animal averages (mean ± s.e.m.), and their facecolor being any other than black indicates that the underlying dilation distribution was significantly shifted from zero (p<0.05, one-sample two-tailed t-test). The gradient bar and arrow symbolize the uneven contribution of the last two sessions to the data pool shown in (D), with the last session contributing the most. (**B**) Time-course of the boundary manipulation experiment. The thin horizontal dotted lines represent the four categorical boundaries animals experienced in these sessions (i.e., boundary changes followed the same rules as the temperature manipulation experiments: a control-manipulation-control 3-min block design with boundaries drawn at random and without replacement from the set B = {1.32, 1.5, 1.68, 1.85} s until exhaustion, at which point the set was replenished and the sampling process resumed). The color scheme introduced in this panel is preserved throughout the figure. (**C**) Same as (A), but for the first five boundary manipulation sessions (N = 5 rats). (**D**) Average discrimination performance on the last and second to last sessions of striatal temperature manipulations. Main axes: psychometric functions fit to cross-animal averages of temperature-split psychophysical data, respectively shown as solid lines and markers of matching color (mean ± s.e.m.). Bottom-right inset: Average differences in proportion of long choices from each manipulation condition to control (mean ± propagated s.e.m.). Top-left inset: Marginal posterior distributions of the threshold parameter for each condition's psychometric fit. Solid black lines represent the M.A.P. point estimates implicit in the fits shown in the main axes. (**E**) Distributions of percentage change in threshold relative to control (dilation) as a function of which categorical boundary was enforced. Markers represent individual threshold dilations, linked within animals by thin solid black lines. (**F**) Same as (D), but for the last two days of boundary manipulations,

with all boundaries in our manipulation set as dotted vertical dashed lines.